CENTRAL RESEARCH LIBRARY

ORNL/TM-5502

Cy 2

MARTIN MARIETTA ENERGY SYSYEMS LIBRARIES

3 4456 0321888 1

Irradiation Performance of HTGR Recycle Fissile Fuel

F. J. Homan
E. L. Long, Jr.

OAK RIDGE NATIONAL LABORATORY
CENTRAL RESEARCH LIBRARY
DOCUMENT COLLECTION
LIBRARY LOAN COPY
DO NOT TRANSFER TO ANOTHER PERSON
If you wish someone else to see this document, send in name with document and the library will arrange a loan.
UCN-7969
(3 3-67)

OAK RIDGE NATIONAL LABORATORY
OPERATED BY UNION CARBIDE CORPORATION FOR THE ENERGY RESEARCH AND DEVELOPMENT ADMINISTRATION

Printed in the United States of America. Available from
National Technical Information Service
U.S. Department of Commerce
5285 Port Royal Road, Springfield, Virginia 22161
Price: Printed Copy $4.50; Microfiche $2.25

This report was prepared as an account of work sponsored by the United States Government. Neither the United States nor the Energy Research and Development Administration/United States Nuclear Regulatory Commission, nor any of their employees, nor any of their contractors, subcontractors, or their employees, makes any warranty, express or implied, or assumes any legal liability or responsibility for the accuracy, completeness or usefulness of any information, apparatus, product or process disclosed, or represents that its use would not infringe privately owned rights.

17-11

ORNL/TM-5502
UC-77 (Gas-Cooled
Reactor Technology)

Contract No. W-7405-eng-26

METALS AND CERAMICS DIVISION

IRRADIATION PERFORMANCE OF HTGR RECYCLE FISSILE FUEL

F. J. Homan and E. L. Long, Jr.

AUGUST 1976

OAK RIDGE NATIONAL LABORATORY
Oak Ridge, Tennessee 37830
operated by
UNION CARBIDE CORPORATION
for the
ENERGY RESEARCH AND DEVELOPMENT ADMINISTRATION

MARTIN MARIETTA ENERGY SYSYEMS LIBRARIES
3 4456 0321888 1

CONTENTS

ABSTRACT 1
INTRODUCTION 1
PERFORMANCE OF DENSE OXIDE KERNELS 2
IRRADIATION PERFORMANCE OF WAR FISSILE FUELS 14
PERFORMANCE OF COATED PARTICLES AND FUEL RODS 35
FUTURE PLANS 38
Product Specification Support 42
Real-Time Testing 42
Advanced Fuels 43
DISCUSSION AND SUMMARY 43
ACKNOWLEDGMENTS 44
REFERENCES 47

IRRADIATION PERFORMANCE OF HTGR RECYCLE FISSILE FUEL

F. J. Homan and E. L. Long, Jr.

ABSTRACT

The irradiation performance of candidate HTGR recycle fissile fuel under accelerated testing conditions is reviewed. Failure modes for coated-particle fuels are described, and the performance of candidate recycle fissile fuels is discussed in terms of these failure modes. The bases on which UO_2 and $(Th,U)O_2$ were rejected as candidate recycle fissile fuels are outlined, along with the bases on which the weak-acid resin (WAR)-derived fissile fuel was selected as the reference recycle kernel. Comparisons are made relative to the irradiation behavior of WAR-derived fuels of varying stoichiometry and conclusions are drawn about the optimum stoichiometry and the range of acceptable values. Plans for future testing in support of specification development, confirmation of the results of accelerated testing by real-time experiments, and improvement in fuel performance and reliability are described.

INTRODUCTION

Irradiation testing of fissile fuels in support of HTGR recycle fuel development[1] has involved three distinct kernel types. They are (1) UO_2, (2) $(Th_{1-z}U_z)O_2$, and (3) a uranium-containing kernel derived from a weak-acid ion exchange resin. This testing was done over a ten-year period and is summarized in ref. 2. This decade of testing has resulted in the identification of five failure mechanisms for coated-particle fuels:

1. "Amoeba" or thermal migration of the kernel up the temperature gradient and through the coating layers.
2. Fission-product attack of the coatings and mechanical interaction of coatings with fission products, usually in combination, which results in ruptured coatings. This problem is most severe in Triso particles, where the SiC layer is attacked.
3. Pressure vessel failure from internal gas pressure and stresses caused by the dimensional changes in the coating, resulting from irradiation damage.
4. Matrix-particle interaction involving a strong bond between the outer coating and the matrix material. Both materials densify under irradiation, resulting in tensile forces that will destroy coating integrity if the bond is not broken first.

+ oxidation of SiC
+ thermal degradation of SiC

5. Fabrication defects or imperfections in the coatings introduced during coating or in subsequent processing.

Of the failure mechanisms listed above, thermal migration and fission product attack of the coatings are related to kernel chemistry. Thermal migration eliminated both UO_2 and $(Th_{1-z}U_z)O_2$ from consideration as fissile recycle fuel. Fission-product attack of the SiC coating eliminated WAR-derived UC_2 kernels. Dense UC_2 kernels were not considered for recycle application, because kernel preparation processes were considered to be too complex for remote operation. Pressure vessel failure, matrix-particle interaction, and fabrication defect failure are not related to kernel chemistry.

No related to MO_2!

This report will discuss only irradiation testing of candidate recycle fissile fuels. Work on process considerations, economics, and thermodynamic analysis is reported elsewhere.[1] Most of the discussion on irradiation performance is associated with coated particles, and, in particular, the kernels. Most of the testing described is with fuel rods made by the slug-injection[3] process, and some aspects of fuel rod performance will be covered.

PERFORMANCE OF DENSE OXIDE KERNELS

The first candidate recycle fuel for the HTGR was UO_2. Early irradiation testing of UO_2 identified a severe problem with thermal migration of the UO_2 kernel up the temperature gradient and through the coating layers. An example of this migration is shown in Fig. 1. The temperature and temperature gradient to which these particles were exposed were nearly equivalent to those in a Large High-Temperature Gas-Cooled Reactor (LHTGR). Representative HTGR temperatures and temperature gradients are provided in Fig. 2 and Table 1.[4,5]

The thermal stability of UO_2 relative to ThO_2 can be seen in Fig. 1. The subject of thermal migration has been extensively studied and documented in the technical literature[6,7] and will not be discussed in depth in this report. Figure 3 compares the average thermal stability of several kernels, among them UO_2 and ThO_2; the upper and lower 90% confidence limits for the data generally lie half an order of magnitude above and below the average. The cross-hatched region and above represents unacceptable performance. This region was determined by calculating the kernel migration coefficients that would lead to migration of the kernel through the buffer layer during normal operation, for different regions of an LHTGR core. Figure 3 shows that the UO_2 curve intersects the cross-hatched region in the temperature range of primary interest for the LHTGR, whereas the ThO_2 curve is well below the cross-hatched area for all temperatures. The UO_2 kernels were therefore rejected from the development program.

Y-120910

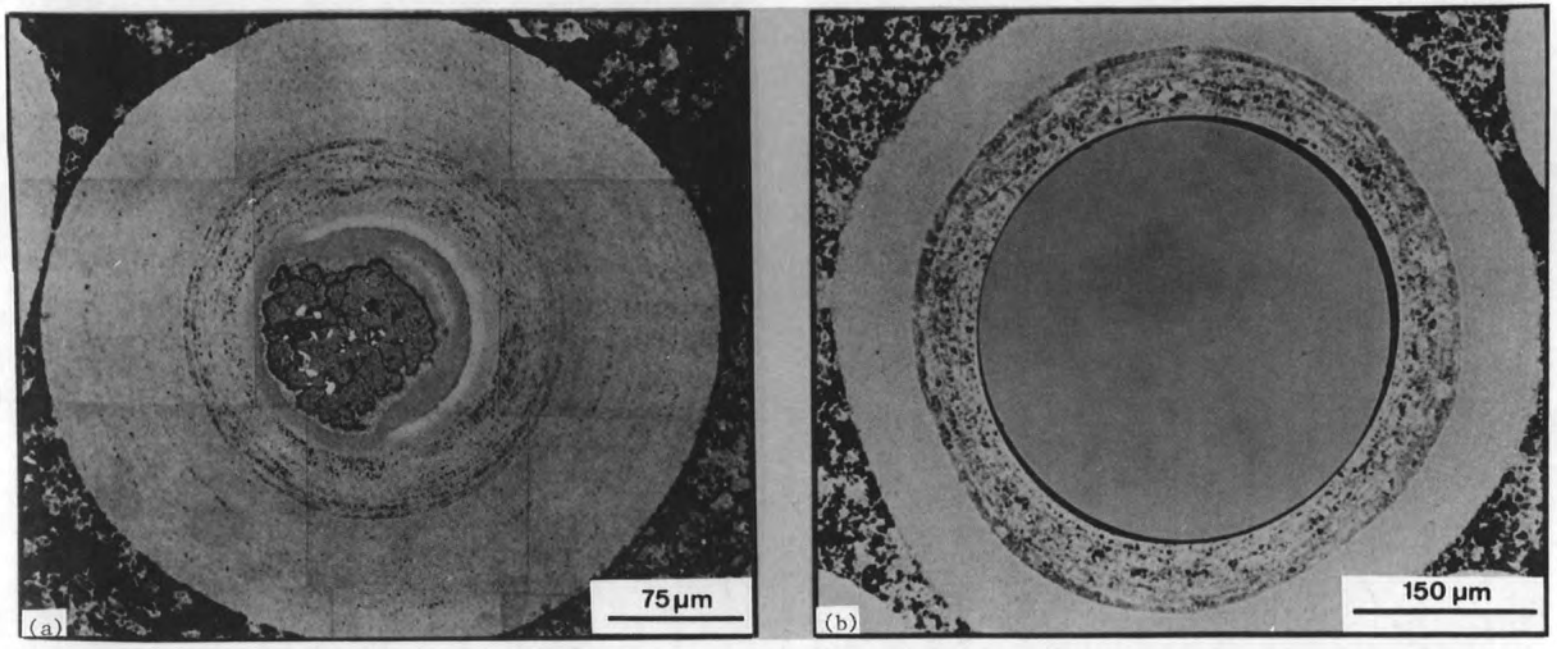

Fig. 1. Relative Thermal Stability of Fissile and Fertile Kernels from Irradiation Test H-1-2. Temperature, 950°C; thermal gradients, 1000°C/cm; fast fluences, 5×10^{21} n/cm^2; time at power, 97 days. (a) UO_2 (33% FIMA). (b) ThO_2 (0.2% FIMA).

higher M_{O_2}
due to fission

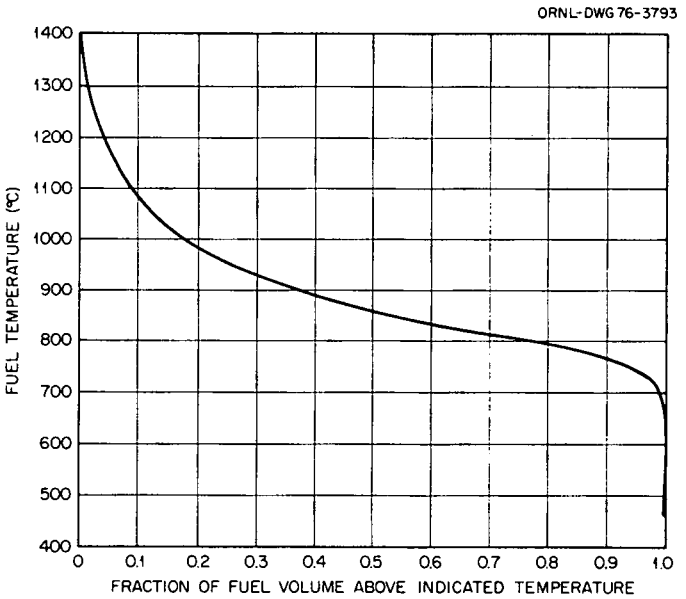

Fig. 2. Fraction of Fuel Operating Above a Given Temperature Under Normal LHTGR Conditions.

Table 1. Comparison of Temperature and Heat Production Parameters for Three Nuclear Power Stations

	Ft. St. Vrain	Summit Station	Fulton Station
Thermal power (MW)	842	2000	3000
Power density (kW/liter)	6.3	8.1	8.4
Fuel rod heat rate (kW/ft)			
Average	1.2	2.3	2.4
Maximum	3.8	6.8	7.0
Heat flux at coolant holes (W/cm^2)			
Average	14.2	20.5	20.5
Maximum	44.2	57.4	58.4
Fuel temperatures (°C)			
Volume average	816	857	890
Maximum (short term)	1260	1420	1410
Hot channel		1585	1571
Graphite temperatures (°C)			
Average	743	777	739
Maximum	1038	1121	1142
Temperature gradients (°C/cm)[a]			
Average		240	250
Maximum		670	700

[a]Based on fuel rod thermal conductivity of 0.07 W cm^{-1}°C^{-1}.

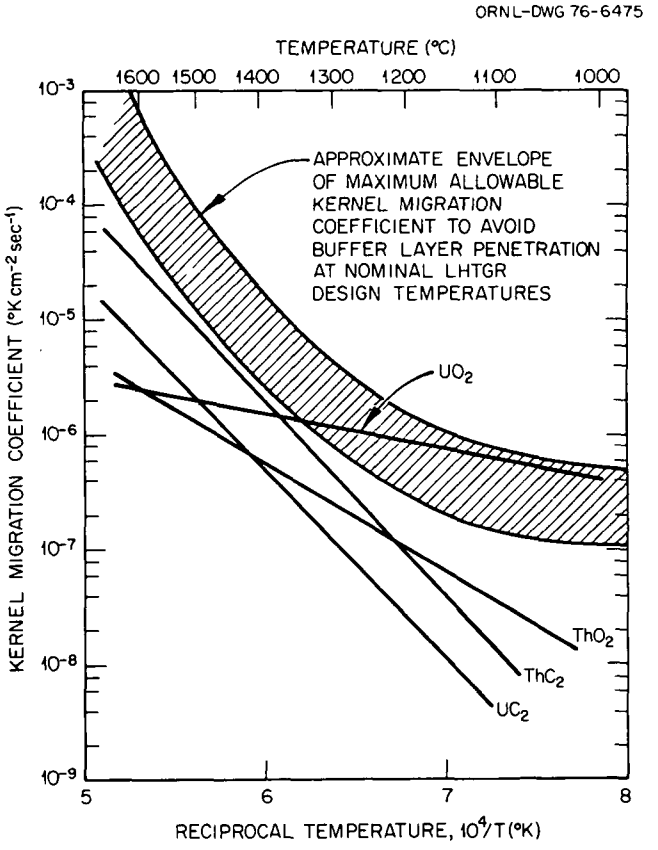

Fig. 3. Average Fuel Kernel Migration Coefficients vs Inverse Temperature Determined From In- and Out-of-Reactor Experiments on Fully Dense Kernels. From D. P. Harmon and C. B. Scott, *Development and Irradiation Performance of LHTGR Fuel*, GA-A13173 (October 1975), p. 103.

The favorable performance of ThO_2 relative to UO_2 suggested dilution of UO_2 with enough ThO_2 for stabilization. Since the overall Th/U ratio in a recycle fuel element is about 8, it appeared as though considerable latitude existed. Mixed thorium-uranium oxide in the ratio of about 4:1 was easy to prepare, and the process was thought to be readily adaptable to the remote operation required in HTGR fuel refabrication. The $(Th_{0.8}U_{0.2})O_2$ kernel was selected as the reference recycle fissile fuel[8] to replace UO_2, and an irradiation program to test the new reference was begun.

A summary of the irradiation testing of the dense mixed-oxide recycle particle is contained in Table 2. Stoichiometries from Th/U = 1 to Th/U = 8 have been tested. Early results at modest irradiation temperatures were encouraging, as shown in Fig. 4 (ref. 9). Very little migration of the $(Th_{0.8}U_{0.2})O_2$ has occurred, and as before, the ThO_2 is very stable. Unfortunately, at higher operating temperatures the $(Th_{0.8}U_{0.2})O_2$ was unstable [Fig. 5 (ref. 10)] where the kernel had migrated through the coatings. Table 2 shows that a significant amount of irradiation data on dense mixed-oxide kernels has been accumulated.

dopants in UO_2

Table 2. Summary of ORNL Experimental Data on Mixed (Th,U) Oxide Recycle Fuel
Part 1. Real-Time Testing Under HTGR Conditions in Peach Bottom Reactor

Irradiation[1,2] experiment No.	Batch No. and fuel type	Th/U ratio	Fast fluence E > 0.18 MeV (n/cm^2)	Average burnup (% FIMA)	Maximum fuel temperature (°C)	Design[a] (μm)	Density[a] (g/cm^3)	Remarks
RTE-1 (FTE-11)								
Body 1	PR-56	4:1	3.3×10^{21}	9.0	c	350/75/130	10.1/1.1/1.9	Slug-injected; carbonized in covered graphite tray; to be examined.
	PR-66	2:1		14.7		350/90/130	10/1.17/1.86	
Body 2	PR-56	4:1		9.0		350/75/130	10.1/1.1.1.9	
	PR-66	2:1		14.7		350/90/130	10/1.17/1.86	
Body 3	PR-56	4:1		9.0		350/75/130	10.1/1.1/1.9	
	PR-67	2:1		14.7		350/90/140	10/1.17/1.85	
Body 4	PR-56	4:1		9.0		350/75/130	10.1/1.1/1.9	
	PR-67	2:1		14.7		350/90/140	10/1.17/1.85	
Body 5	PR-66	2:1		14.7		350/90/130	10/1.17/1.86	
Body 6	PR-66	2:1		14.7		350/90/130	10/1.17/1.86	
RTE-2								
Body 2	PR-66	2:1	3.6×10^{21}	13.3	1190[d]	350/90/130	10/1.17/1.86	Slug-injected; carbonized in covered graphite tray. Fuel examined from highest temperature region and is considered representative; no amoeba; no indication of failure.
Body 5	PR-55	4:1	3.6×10^{21}	8.2	1300[d]	350/70/80	10.1/1.1/1.9	Loose bed of particles; fuel examined from highest temperature region and is considered representative; no amoeba; no indication of failure.
RTE-4								
Body 3	PR-54	4:1	2.0×10^{21}	5.0	1260[d]	350/70/70	10.1/1.1/1.94	Loose bed of particles; fuel examined from highest temperature region and is considered representative; no amoeba; no indications of failure.
Body 5	PR-61	2:1	2.0×10^{21}	8.5	1230[d]	350/75/120	10.2/1.16/1.91	Slug-injected; carbonized in covered graphite tray; fuel examined from highest temperature region and is considered representative; no amoeba; no indication of failure.
RTE-5								
Body 1	PR-57-1	4:1	4.6×10^{21}	11.9	c	350/75/135	10.1/1.1/1.9	Slug-injected; carbonized in covered graphite tray; to be examined.
	PR-61	2:1		18.4		350/75/120	10.2/1.16/1.9	
Body 2	PR-57-1	4:1		11.9		350/75/135	10.1/1.1/1.9	
	PR-61	2:1		18.4		350/75/120	10.2/1.16/1.9	
Body 3	PR-57-1	4:1		11.9		350/75/135	10.1/1.1/1.9	
	PR-61	2:1		18.4		350/75/120	10.2/1.16/1.9	
Body 4	PR-57-1	4:1		11.9		350/75/135	10.1/1.1/1.9	
	PR-61	2:1		18.4		350/75/120	10.2/1.16/1.9	
Body 5	PR-60	2:1		18.4		350/75/120	10.2/1.16/1.9	
Body 6	PR-60	2:1		18.4		350/75/120	10.2/1.16/1.9	
RTE-6								
Body 3	PR-60	2:1	4.6×10^{21}	18.2	c	350/75/120	10.2/1.16/1.9	Slug-injected;carbonized in covered graphite tray; fuel examined from highest temperature region and is considered representative; no amoeba; no indication of failure.
RTE-8								
Body 4	PR-60	2:1	4.6×10^{21}	18.1	c	350/75/120	10.2/1.16/1.9	Slug-injected; carbonized in covered graphite tray.
RTE-7								
Body 1	PR-60	2:1	1.3×10^{21}	5.5	880[d]	350/75/120	10.2/1.16/1.9	Slug-injected; carbonized in covered graphite tray; fuel examined from highest temperature region and is considered representative; no amoeba; no indications of failure.
Body 2	PR-60	2:1		5.5	1130[d]	350/75/120	10.2/1.16/1.9	
Body 3	PR-60	2:1		5.5	1230[d]	350/75/120	10.2/1.16/1.9	
Body 4	PR-60	2:1		5.5	1230[d]	350/75/120	10.2/1.16/1.9	
Body 5	PR-57-1	4:1		3.2	1150[d]	350/75/135	10.1/1.1/1.9	
	PR-57-6	4:1		3.2	1150[d]	350/75/135	10.1/1.1/1.9	
	PR-61	2:1		5.5	1150[d]	350/75/120	10.2/1.16/1.9	
Body 6	PR-57-1	4:1		3.2	1050[d]	350/75/135	10.1/1.1/1.9	
	PR-61	2:1		5.5	1050[d]	350/75/120	10.2/1.16/1.9	

Part 2. Accelerated Testing in Research Reactors

Fissile particle batch No.	Sample identification	Fast fluence E > 0.18 MeV (n/cm^2)	Burnup (% FIMA)	Th/U Ratio	Design A/B/C/D/E (μm)	Density A/B/C/D/E (μm)	Maximum fuel temperature (°C)
				H-1[3]			
PR-57	H-1-4	6.3×10^{21}	8.2	4:1	355/80/135	10.1/1.1/1.92	1420[e]
	H-1-10	5.4	8.6	4:1	355/80/135	10.1/1.1/1.92	2150[e]
	H-1-6	8.6	8.6	4:1	355/80/135	10.1/1.1/1.92	1670[e]
PR-67	H-1-3	5.8×10^{21}	12.0	2:1	350/80/140	10/1.1/1.85	1370[e]
	H-1-11	4.5	12.0	2:1	350/80/140	10/1.1/1.85	2390[e]
				H-2[7]			
PR-57	H-2-4	7.5×10^{21}	7.5	4:1	355/80/135	10.1/1.1/1.92	1430[e]
	H-2-10	8.3	8.3	4:1	355/80/135	10.1/1.1/1.92	1800[e]
	H-2-6	8.2	8.2	4:1	355/80/135	10.1/1.1/1.92	1690[e]
PR-67	H-2-3	5.2×10^{21}	11.0	2:1	350/80/140	10/1.1/1.85	1350[e]
	H-2-11	4.1	12.0	2:1	350/80/140	10/1.1/1.85	1910[e]
				HRB-1[4]			
YZ-233	1A	2.9×10^{21}	9.8	4:1	195/37/20/33/53	3.4/?/?/3.11/1.8	
	1B	2.9	9.8		195/37/20/33/53		
	1C	2.9	9.8		195/37/20/33/53		770[f]
	2A	3.4	10.2		195/37/20/33/53		
	3A	4.8	12.7		195/37/20/33/53		
	3B	4.8	12.7		195/37/20/33/53		1150[f]
	4A	5.3	13.8		195/37/20/33/53		1400[f]
	5A	5.8	14.9		195/37/20/33/53		1130[f]
	5B	5.8	14.9		195/37/20/33/53		
	6A	5.4	14.0		195/37/20/33/53		
	6B	5.4	14.0		195/37/20/33/53		1140[f]
				HRB-6[5]			
OR-1910	1A	5.8×10^{21}	23.8	4:1	350/100/30/25/40	10/1.15/1.95/3.2/1.95	
OR-1909	1B	6.8	25.8		350/100/30/25/40	10/1.15/1.95/3.2/1.95	1190[g]
PU-291	3A	7.2	26.7		350/100/80	10/1.15/1.95	1220[g]
OR-1909	3B	6.7	26.0		350/100/90	10/1.15/1.95	1200[g]
Pu-291	3C	6.1	25.0		350/100/80	10/1.15/1.95	1300[g]
OR-1909	3D	5.4	23.6		350/100/90	10/1.15/1.95	1250[g]
				HRB-7[6,7]			
J-263	2	4.07×10^{21}	20.8	4:1	350/100/100	10/1.3/2.0	1500[h]
OR-2094H	8	6.04	32.8	2:1	300/85/85	10/1.2/1.95	
OR-2116H	9	6.14	22.5	4:1	350/100/30/30/40	10/1.2/1.95/3.18/1.95	
GGA-6155-01-020	10	6.14	16.4	8:1	500/100/30/30/40	10/1.2/1.95/3.18/1.8	
OR-2111H	11	6.14	21.7	4:1	350/90/100	10/1.2/2.00	
OR-2090H	12	6.04	43.9	1:1	250/85/85	10/1.2/1.95	
J-263	19	3.62	18.9	4:1	350/100/100	10/1.3/2.0	
				HRB-8[6,7]			
J-263	2	5.35×10^{21}	21.4	4:1	350/100/100	10/1.3/2.0	1250[h]
OR-2094-H	8	7.95	34.0	2:1	350/85/85	10/1.2/1.95	
OR-2116-H	9	8.09	25.3	4:1	350/100/30/30/40	10/1.2/1.95/3.18/1.95	
GGA-6155-01-0RO	10	8.09	19.4	8:1	500/100/30/30/40	10/1.2/1.95/3.18/1.8	
OR-2111-H	11	8.09	24.6	4:1	350/90/100	10/1.2/2.00	
OR-2090-H	12	7.95	45.7	1:1	250/85/85	10/1.2/1.95	
J-263	19	4.78	18.8	4:1	350/100/100	10/1.3/2.0	
				HRB-9[6]			
OR-2116H	2	5.25×10^{21}	21.2	4:1	350/100/30/30/40	10/1.2/1.95/3.18/1.95	1250[h]
OR-2116H	7	7.57	24.4	4:1	350/100/30/30/40	10/1.2/1.95/3.18/1.95	1250[h]
				HRB-10[6]			
OR-2116H	2	3.3×10^{21}	18.4	4:1	350/100/30/30/40	10/1.2/1.95/3.18/1.95	1500[h]
OR-2116H	7	4.8	20.5	4:1	350/100/30/30/40	10/1.2/1.95/3.18/1.95	1500[h]
				OF-1[7]			
J-263	Rod 1-1	10.8×10^{21}	19.0	4.2:1	350/100/100	10/1.1/2.0	1200[h]
	1-2	9.58	18.1				
	1-3	8.00	16.9				
	1-4	5.72	15.9				
J-263	2-1	9.85	18.3				
	2-2	8.61	17.5				
	2-3	6.99	16.4				
	2-4	4.88	15.5				
OR-1977	3-1	9.85	16.9				
OR-1977	3-2	8.61	16.1				
J-263	3-3	7.40	16.7				
J-263	3-4	5.92	16.0				
J-263	3-5	4.37	15.3				
J-263	4-1	10.8	19.0				
	4-2	9.58	18.1				
	4-3	8.00	16.9				
	4-4	5.72	15.9				
Pu 291[a]	5-1	10.4	20.2[a]				
OR 1977	5-2	9.18	16.4				1350[h]
Pu 291[a]	5-3	7.48	18.1[a]				1350[h]
OR 1977	5-4	5.25	14.4				1350[h]

Part 2a. Accelerated Testing in Research Reactors

Fissile particle batch No.	Sample identification	Remarks
		H-1
PR-57	H-1-4	Only failures noted in single plane of polish viewed were due to fabrication defects.
	H-1-10	Very high temperatures during fourth cycle; extensive damage at center of rod.
	H-1-6	Loose particles. Amoeba related failures.
PR-67	H-1-3	Only slight evidence of amoeba; no failed coatings.
	H-1-11	Rod debonded into large fragments; damaged particles on surface of rod.
		H-2
PR-57	H-2-4	Not examined; sent to Chemical Technology Division for reprocessing studies.
	H-2-10	Center badly damaged due to very high temperature during last cycle.
	H-2-6	Loose particles. Not examined.
PR-67	H-2-3	Fuel rod debonded; no failed particles observed during visual examination.
	H-2-11	Outer surfaces of particles near the surface of rod chemically attacked; amoeba apparent; kernel migrated through buffer and into LTI.
		HRB-1
YZ-233	1A	Slug-injected rods; thin two-component sacrificial layer on outer surface of particles caused debonding of rods with low-density matrix (1A, 1B, 1C, 2A, 4A, 4B). Metallography showed no failed particles or amoeba.
YZ-233	1B	
YZ-233	1C	
YZ-233	2A	
YZ-233	3A	
YZ-233	3B	
YZ-233	4A	
YZ-233	5A	
YZ-233	5B	
YZ-233	6A	
YZ-233	6B	
		HRB-6
OR-1910	1A	Extruded rod; no failures; no amoeba; intermittent plastic flow through recoil zone.
OR-1909	1B	Extruded rod; no failures; slight amoeba (2–3 μm); intermittent plastic flow through recoil zone.
Pu-291*	3A	Slug-injected; carbonized in packed Al_2O_3; > 50% failed; amoeba (20 μm); failures attributed to defective coatings.
OR-1909	3B	Slug-injected; carbonized in packed Al_2O_3; no failures; amoeba (20 μm).
Pu-291*	3C	Slug-injected; carbonized in packed Al_2O_3; visual examination only; no broken particles.
OR-1909	3D	Slug-injected; carbonized in packed Al_2O_3; visual examination only; no broken particles.
		HRB-7
J-263	2	Slug-injected; carbonized in packed Al_2O_3; no failures; amoeba (≤ 40 μm).
OR-2094H	8	Slug-injected; carbonized in packed Al_2O_3; no failures; amoeba (≤ 80 μm).
OR-2116H	9	Slug-injected; carbonized in packed Al_2O_3; no failures; amoeba (≤ 25 μm).
GGA-6155-01-020	10	Slug-injected; carbonized in packed Al_2O_3; 12% failed; amoeba (≤ 25 μm).
OR-2111H	11	Slug-injected; carbonized in packed Al_2O_3; no failures; amoeba (≤ 75 μm).
OR-2090H	12	Slug-injected; carbonized in packed Al_2O_3; no failures; amoeba (≤ 55 μm).
J-263	19	Slug-injected; carbonized in packed Al_2O_3; no failures; amoeba (≤ 30 μm).
		HRB-8
J-263	2	Slug-injected; carbonized in packed Al_2O_3; no failures; amoeba (≤ 13 μm).
OR-2094-H	8	Slug-injected; carbonized in packed Al_2O_3; no failures; amoeba (≤ 20 μm).
OR-2116-H	9	Slug-injected; carbonized in packed Al_2O_3; no failures; amoeba (≤ 25 μm).
GGA-6155-01-020	10	Slug-injected; carbonized in packed Al_2O_3; no failures; amoeba (≤ 85 μm).
OR-2111-H	11	Slug-injected; carbonized in packed Al_2O_3; no failures; amoeba (≥ 20 μm).
OR-2090-H	12	Slug-injected; carbonized in packed Al_2O_3; 13% failed; amoeba (≤ 55 μm).
J-263	19	Slug-injected; carbonized in packed Al_2O_3; no failures; amoeba (≤ 20 μm).

Part 2a. Accelerated Testing in Research Reactors (Continued)

Fissile particle batch No.	Sample identification	Remarks
		HRB-9
OR-2116H	2	Slug-injected; carbonized in packed Al_2O_3; visual examination only; no broken particles.
OR-2116H	7	Slug-injected; carbonized in packed Al_2O_3; visual examination only; no broken particles.
		HRB-10
OR-2116H	2	Slug-injected; carbonized in packed Al_2O_3; visual examination only; no broken particles.
OR-2116H	7	Slug-injected; carbonized in packed Al_2O_3; no failures; amoeba ($\leq$ 35 μm).
		OF-1
J-263	1-1	Slug-injected; no failures (Metallography); amoeba ($\leq$ 5 μm); carbonized in packed Al_2O_3.
	1-2	Slug-injected; stereo-examination only; no broken particles; carbonized in packed Al_2O_3.
	1-3	Slug-injected; stereo-examination only; no broken particles; carbonized in packed Al_2O_3.
	1-4	Slug-injected; stereo-examination only; no broken particles; carbonized in packed Al_2O_3.
J-263	2-1	Slug-injected; stereo-examination only; no broken particles; carbonized in graphite block.
	2-2	Slug-injected; no failures (Metallography); amoeba ($\leq$ 5 μm); carbonized in graphite block.
	2-3	Slug-injected; stereo-examination only; no broken particles; carbonized in graphite block.
	2-4	Slug-injected; stereo-examination only; no broken particles; carbonized in graphite block.
OR-1977	3-1	Slug-injected; stereo-examination only; no broken particles; carbonized in packed Al_2O_3.
OR-1977	3-2	Slug-injected; no failures (Metallography); amoeba ($\leq$ 20 μm); carbonized in packed Al_2O_3.
J-263	3-3	Slug-injected; stereo-examination only; no broken particles; carbonized in packed Al_2O_3.
J-263	3-4	Slug-injected; no failures (Metallography); no amoeba; carbonized in packed Al_2O_3.
J-263	3-5	Slug-injected; stereo-examination only; no broken particles; carbonized in packed Al_2O_3.
J-263	4-1	Slug-injected; no failures (Metallography); amoeba ($\leq$ 20 μm); carbonized in graphite block.
J-263	4-2	Slug-injected: stereo-examination only; 3 broken particles on surface (identity unknown); carbonized in graphite block.
J-263	4-3	Slug-injected; stereo-examination only; no broken particles; carbonized in graphite block.
J-263	4-4	Slug-injected; stereo-examination only; no broken particles; carbonized in graphite block.
Pu-291[i]	5-1	Slug-injected; ~ 80% failed (Metallography); carbonized in packed Al_2O_3; ($\leq$ 15 μm); failures attributed to defective coatings.
OR-1977	5-2	Slug-injected; no failures (Metallography) carbonized in packed Al_2O_3; no amoeba.
Pu-291[i]	5-3	Slug-injected; ~ 15% failed (Metallography); carbonized in packed Al_2O_3; amoeba (< 10 μm); failures attributed to defective coatings.
OR-1977	5-4	Slug-injected; stereo-examination only; carbonized in packed Al_2O_3; no broken particles.

[a]A = kernel; B = buffer; C = IPyC; D = SiC; E = OPyC.

[b]Approximately 11,000 to 18,000 fissile particles per rod in RTE fuel rods, depending on particle diameter and density. Forty-eight fuel rods per body.

[c]Thermal analysis to be completed by July 1976.

[d]Maximum fuel temperature in fuel body. These are estimated temperatures based on as-fabricated dimensions. Detailed analyses incorporating irradiation-induced dimensional changes are being performed.

[e]These temperatures represent the maximum calculated for the fuel rod centerline during the irradiation. This experiment was complicated by a nonintentional inversion of the capsule during the last of four irradiation cycles. (See ref. 4 for additional details on fuel operating temperatures.)

[f]Temperatures for HRB-1 were calculated from readings from thermocouples adjacent to fuel rods. Centerline temperatures were calculated by assuming a fuel rod conductivity of 3.0 Btu/hr-ft-°F and a radial gap of 0.004 in. Fuel rod 4B was composed of a resin binder, and the matrix debonded rather badly during irradiation. Therefore, the thermal conductivity of the fuel rod may have been as low as 1.5 Btu/hr-ft-°F (a value associated with loose beds of particle). This change in the bed conductivity increases the calculated fuel centerline temperature from 1230 to 1430°C.

[g]From detailed thermal analysis (ref. 5).

[h]Maximum design fuel temperatures.

[i]Fueled with ^{233}U.

References

[1]E. L. Long, Jr. et al., *Fabrication of ORNL Fuel Irradiated in the Peach Bottom Reactor and Postirradiation Examination of Recycle Test Elements 7 and 4*, ORNL-TM-4477 (September 1974).

[2]R. P. Morissette and K. P. Steward, *Recycle Test Element Program Design, Fabrication, and Assembly*, GA-10109 (September 1971).

[3]R. A. Olstad et al., *An Irradiation Test of Candidate HTGR Recycle Fuels in the H-1 and H-2 Capsules*, ORNL-TM-4397 (July 1974).

[4]J. L. Scott et al., *An Irradiation Test of Bonded HTGR Coated Particle Fuels in an Instrumented Capsule in HFIR*, ORNL-TM-3640 (March 1972).

[5]F. J. Homan et al., *Irradiation Performance of HTGR Fuel Rods in HFIR Experiment HRB-6*, ORNL-TM-5011 (December 1975).

[6]K. H. Valentine et al., *Irradiation Performance of HTGR Fuel Rods in HFIR Experiments in HRB-7 and -8*, in preparation.

[7]*HTGR Base Program Progr. Rep. Jan. 1, 1974 to June 30, 1975*, ORNL-5108, in preparation.

Y-120917

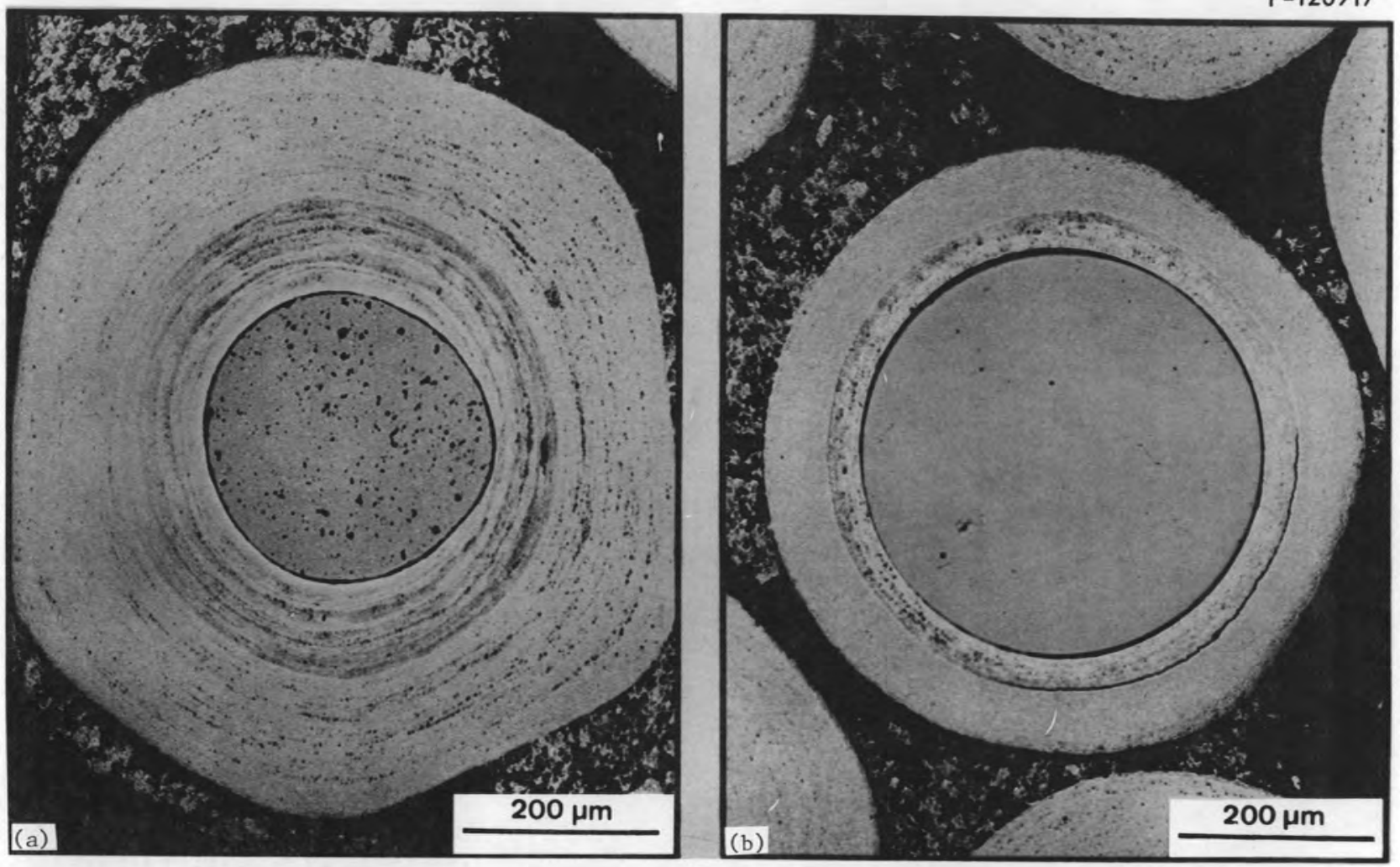

Fig. 4. Relative Thermal Stability of Fissile and Fertile Particles in Irradiation Test H-1-4. Temperature, 1050°C; thermal gradient, 1200°C/cm; fast fluence, 6.3×10^{21} n/cm^2; time at power, 134 days. (a) (4.1 Th,U)O_2 (8.2% FIMA). (b) ThO_2 (0.4% FIMA).

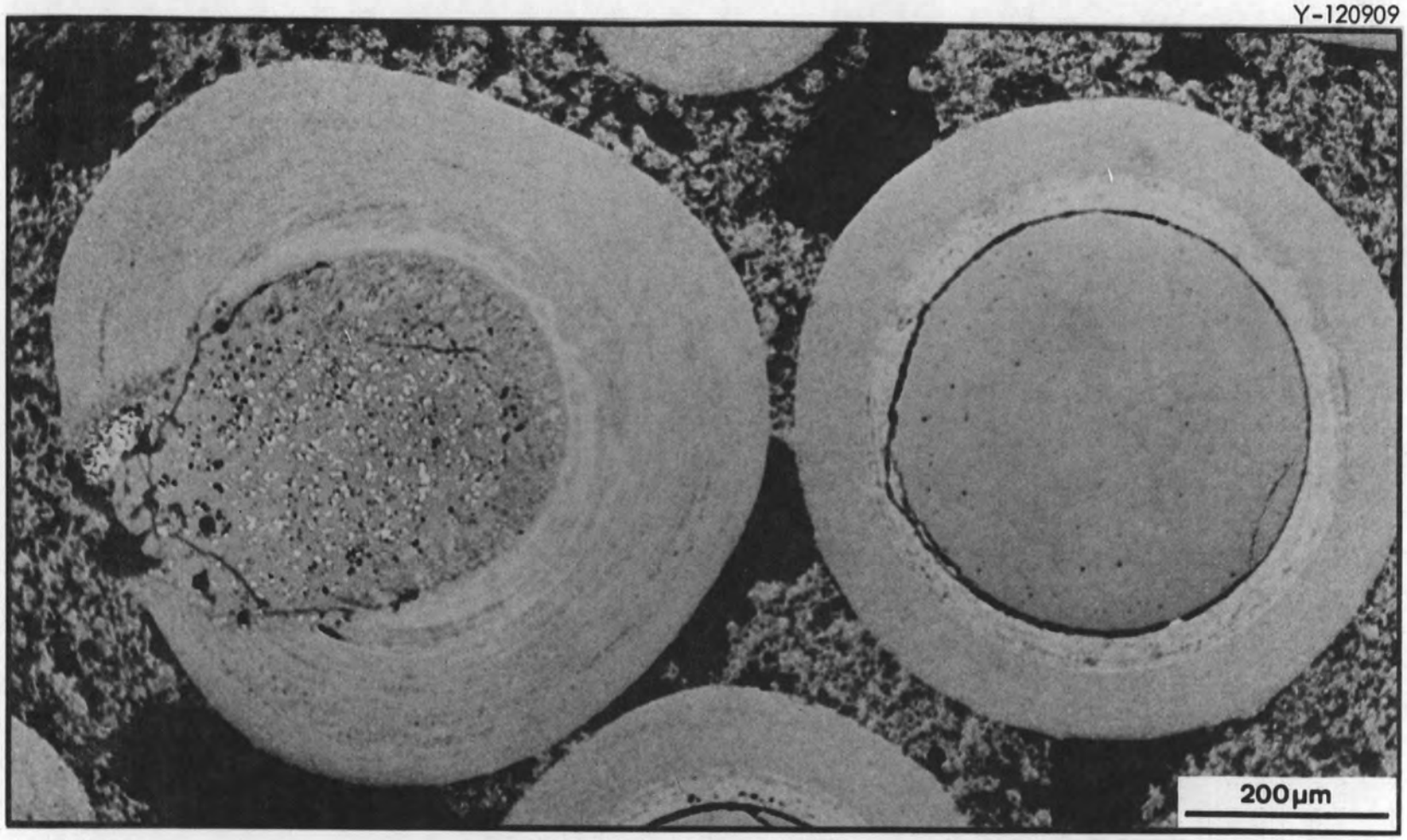

Fig. 5. Relative Thermal Stability of Fissile and Fertile Kernels in Irradiation Test H-2-10. Temperature, 1350°C; thermal gradient, 1700°C/cm; fast fluence, 5×10^{21} n/cm^2; time at full power, 37 days. Left: (4 Th,U)O_2 (8.3% FIMA). Right: ThO_2 (0.3% FIMA).

These data were treated in similar fashion to the UO_2 and ThO_2 data shown in Fig. 3. The results are given in Fig. 6. The average curve for $(Th_{0.8}U_{0.2})O_2$ falls at the bottom of the cross-hatched critical region in the temperature range 1100–1400°C. However, when the scatter of the thermal migration data is taken into account and the 90% confidence intervals are plotted, the upper confidence interval curve extends well into the cross-hatched region. This treatment of the irradiation data for the reference recycle kernel led to the conclusion that this fuel had marginal thermal stability, and an alternate reference fissile fuel was sought. At this stage, additional irradiation testing of other stoichiometries was under way;[11] however, the results showed little improvement over the reference (Th/U = 4) system. A summary of the data from the High Flux Isotope Reactor (HFIR) removable beryllium (HRB)-7 capsule[11] for fuels with Th/U ranging from 0 to 8 is shown in Fig. 7. The thermal stability improves with the addition of thorium to the kernels, but the stability of $(Th_{0.89}U_{0.11})O_2$ is about the same as $(Th_{0.8}U_{0.2})O_2$.[9]

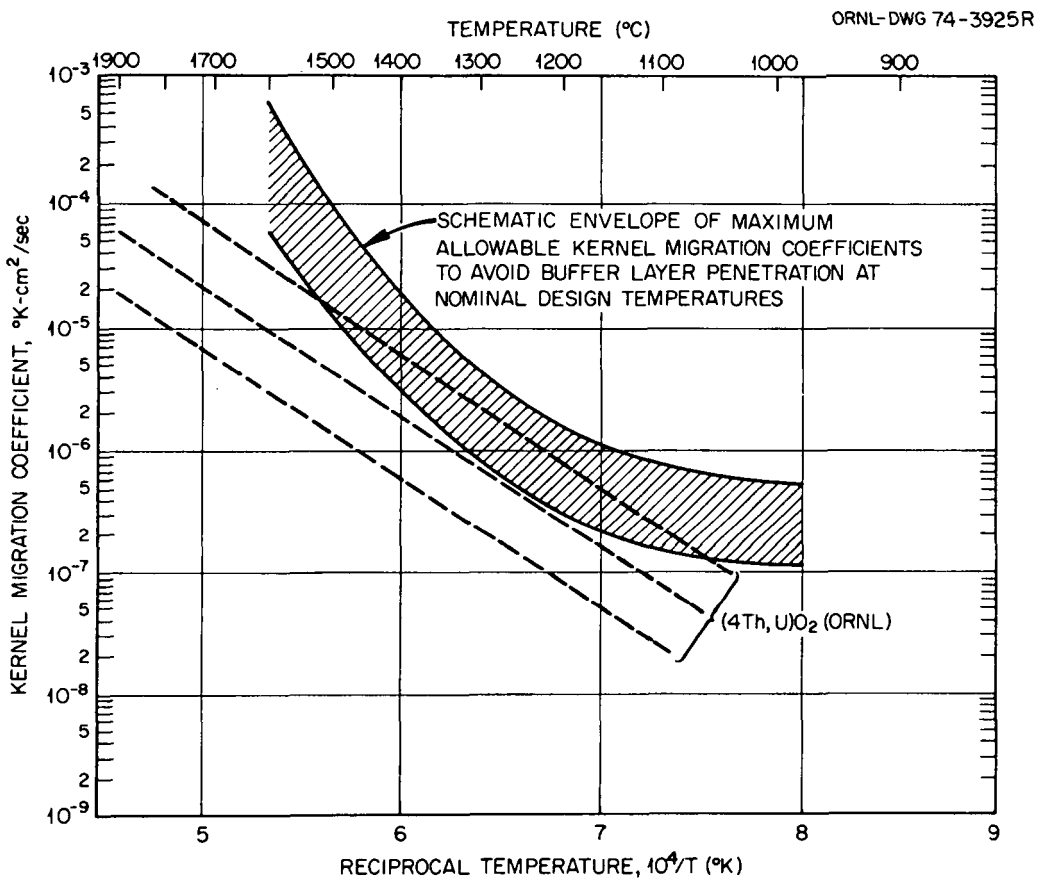

Fig. 6. Average Kernel Migration Coefficients vs Reciprocal Temperature for $(4\ Th,U)O_2$.

R-71120

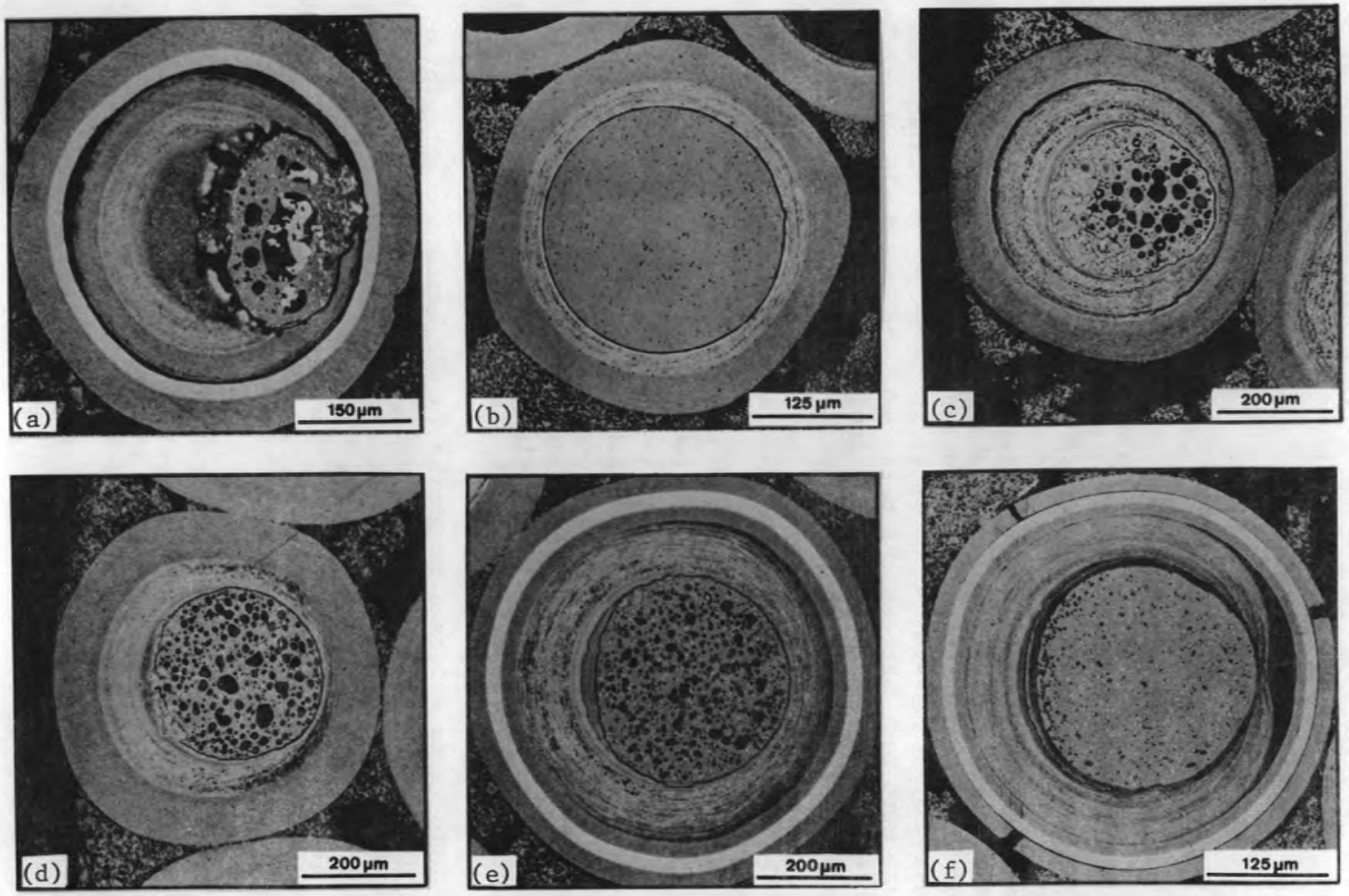

Fig. 7. Relative Thermal Stability of HTGR Candidate Recycle Oxide Fuel Kernels Irradiated in HRB-7. Time-average temperature, 1200–1220°C; thermal gradient, 1000–1030°C/cm; fast fluence, 6×10^{21} n/cm^2. (a) UO_2 (79.8% FIMA). (b) ThO_2 (8.3% FIMA). (c) $(Th,U)O_2$ (43.9% FIMA). (d) $(2\ Th,U)O_2$ (32.0% FIMA). (e) $(4\ Th,U)O_2$ (22.5% FIMA). (f) $(8\ Th,U)O_2$ (16.5% FIMA).

The fissile particle selected to replace the dense mixed oxide was an undiluted fissile kernel (containing only a fissile isotope) derived from loading uranium into ion-exchange resins from a weak-acid solution. WAR-derived fuel will be discussed in detail in the next section.

IRRADIATION PERFORMANCE OF WAR FISSILE FUELS

A summary of the irradiation testing of WAR fuels at ORNL is contained in Table 3. The decision to switch from $(Th_{0.8}U_{0.2})O_2$ to WAR-derived uranium oxide-carbide as the reference recycle fissile kernel was based on the performance of WAR-derived fuel in the HRB-4 and -5 capsules.[12] Typical postirradiation metallography of the WAR fuel irradiated in those capsules is shown in Figs. 8 and 9. Extensive testing of WAR-derived fuels was conducted in capsules HRB-7 and -8 and capsules HRB-9 and -10.[11,13] In these last four capsules, direct comparisons were made between the performance of WAR fuels of various stoichiometries and dense mixed-oxide fuels, as well as with the reference HTGR fresh fuel (dense UC_2).

Several observations have been made about WAR fuel performance from this accelerated testing:

1. The porous WAR kernels densify considerably under irradiation, as shown in Fig. 8. The density of the WAR kernels is typically about 3 g/cm^3 before irradiation, compared with densities greater than 10 g/cm^3 for the dense mixed-oxide kernels described earlier. Frequently, the densified WAR kernels remain attached to one side of the coating layers, as shown in Fig. 8. There is no correlation between temperature gradient and the orientation of the densified kernel.

2. There is no evidence of amoeba in WAR kernels containing more than 15% carbide — with the balance oxide. However, WAR UO_2 kernels have been observed to migrate up the temperature gradient, like the dense oxide kernels described earlier. This can be seen in Fig. 10 in the upper left. Figure 10 summarizes the results of all WAR stoichiometries tested to date. These will be discussed in more detail later in the report.

3. Phase segregation is associated with WAR kernels after irradiation and is more extensive in the lower conversion levels.* Segregation is shown in the lower left portion of Fig. 10 and in Figs. 11 and 12, which will be described in more detail later.

---

*Conversion is from UO_2 to UC_2. In the WAR uranium oxide-carbide kernel, the percent conversion refers to the proportion of UC_2 in the two-phase system; 0% conversion is UO_2, 15% conversion is 85% UO_2 and 15% UC_2, etc.

Table 3. Summary of ORNL Experimental Data on Irradiated Weak-Acid Resin-Derived Recycle Fuel

Fissile particle batch No.	Number of particles irradiated	Sample identification	Fast fluence E > 0.18 MeV (n/cm^2)	Burnup (% FIMA)	Resin	Conversion[a] (%)	Design[b] A/B/C/D/E (um)	Density[b] A/B/C/D/E (g/cm^3)	Maximum fuel[c] temperature (°C)
						HRB-5[(1)]			
52A	5750	1A	3.4×10^{21}	13	IRC-72	95	350/40/30/30/30	6/1.1/1.9/3.18/1.85	1250
	5840	1B	4.0	14					
	5900	1C	4.5	16					
	2950	3A	4.2	15					
	2950	3B	3.9	14					
	2950	3C	3.6	13					
	2950	3D	3.2	12					
						HRB-4[(1)]			
52A	5750	1A	7.8	24	IRC-72	95	350/40/30/30/30	6/1.1/1.9/3.18/1.85	1250
	5840	1B	9.2	27					
	5900	1C	10.3	29					
	2950	3A	9.6	27					
	2950	3B	8.9	25					
	2950	3C	8.1	23					
	2950	3D	7.2	20					
						HRB-6[(2)]			
Pu-295B	28	1C4	7.7	84	IRC-72	?	400/35/25/30/25	3.2/1.2/1.95/3.18/1.95	1250
Pu-296	25	1C5	7.7	84	IRC-72	95	400/35/25/30/25	3.8/1.2/1.95/3.18/1.95	
Pu-297	22	1C6	7.7	84	IRC-72	95	400/35/25/30/25	3.7/1.2/1.95/3.18/1.95	
						HRB-7[(3)]			
OR-2115H	402	13	5.9	80.0	IRC-72	14	400/40/30/30/40	3.2/1.2/1.95/3.18/1.95	1500
OR-2121H	407	14	5.6	79.9	IRC-72	92	300/75/30/30/40	5.3/1.2/1.95/3.18/1.95	
OR-2115H	476	15	5.3	79.9	IRC-72	14	400/40/100	3.2/1.2/1.95	
OR-2121H	511	16	4.9	79.9	IRC-72	92	300/75/85	5.3/1.2/1.95	
						HRB-8[(3)]			
OR-2121H	402	13	7.7	80.4	IRC-72	14	400/40/30/30/40	3.2/1.2/1.95/3.18/1.95	1250
OR-2115H	407	14	7.4	80.3	IRC-72	92	300/75/30/30/40	5.3/1.2/1.95/3.18/1.95	
OR-2121H	476	15	6.9	80.3	IRC-72	14	400/40/100	3.2/1.2/1.95	
OR-2115H	511	16	6.4	80.3	IRC-72	92	300/75/85	5.3/1.2/1.95	
						HRB-9[(4)]			
OR-2208H	593	1	4.7	79.1	IRC-72	100	360/50/30/30/40	3.0/1.2/1.95/3.18/1.95	1250
OR-2121H	433	3	5.8	79.5		100	300/75/30/30/40	5.3/1.2/1.95/3.18/1.95	
OR-2218H	486	4	6.3	79.4		0	360/50/30/30/40	3.7/1.2/1.95/3.18/2.00	
OR-2208H	490	5	6.8	79.9		100	360/50/30/30/40	3.0/1.2/1.95/3.18/1.95	
OR-2115H	373	8	7.8	80.1		15	400/40/30/30/40	3.2/1.2/1.95/3.18/1.95	
OR-2207H	486	9	7.9	80.1		75	360/50/30/30/40	3.0/1.2/1.95/3.18/1.95	
OR-2207H	486	10	7.9	80.1		75	360/50/30/30/40	3.0/1.2/1.95/3.18/1.95	
OR-2208H	469	11	7.9	80.1		100	360/50/30/30/40	3.0/1.2/1.95/3.13/1.95	
OR-2218H	423	12	7.8	80.1		0	360/50/30/30/40	3.7/1.2/1.95/3.18/2.00	
OR-2211H	520	13	7.6	80.0		50	360/50/30/30/40	3.1/1.2/1.95/3.18/2.00	
OR-2121H	398	14	7.2	79.9		100	300/75/30/30/40	5.3/1.2/1.95/3.18/1.95	
OR-2207H	510	15	6.8	79.9		75	360/50/30/30/40	3.0/1.2/1.95/3.18/1.95	
OR-2115H	427	16	6.3	80.0		15	400/40/30/30/40	3.2/1.2/1.95/3.18/1.95	
OR-2211H	566	17	5.8	79.5		50	360/50/30/30/40	3.1/1.2/1.95/3.18/2.00	
OR-2219H	584	18	5.3	79.3		NA	360/50/30/30/40	3.0/1.2/1.95/3.18/2.00	
OR-2207H	616	19	4.7	79.1		75	360/50/30/30/40	3.0/1.2/1.95/3.18/1.95	
OR-2219H	484	6	7.2	80.0		NA	360/50/30/30/40	3.0/1.2/1.95/3.18/2.00	
						HRB-10[(4)]			
OR-2208H	593	1	3.0	77.3	IRC-72	100	360/50/30/30/40	3.0/1.2/1.95/3.18/1.95	1500
OR-2121H	433	3	3.7	78.5		100	300/75/30/30/40	5.3/1.2/1.95/3.18/1.95	
OR-2218H	486	4	4.0	79.2		0	360/50/30/30/40	3.7/1.2/1.95/3.18/2.00	
OR-2208H	490	5	4.3	79.2		100	360/50/30/30/40	3.0/1.2/1.95/3.18/1.95	
OR-2115H	373	8	4.9	79.5		15	400/40/30/30/40	3.2/1.2/1.95/3.18/1.95	
OR-2207H	486	9	5.0	79.6		75	360/50/30/30/40	3.0/1.2/1.95/3.18/1.95	
OR-2207H	486	10	5.0	79.6		75	360/50/30/30/40	3.0/1.2/1.95/3.18/1.95	
OR-2208H	469	11	5.0	79.6		100	360/50/30/30/40	3.0/1.2/1.95/3.18/1.95	
OR-2218H	423	12	4.9	79.5		0	360/50/30/30/40	3.7/1.2/1.95/3.18/2.00	
OR-2211H	520	13	4.8	79.4		50	360/50/30/30/40	3.1/1.2/1.95/3.18/2.00	
OR-2121H	398	14	4.6	79.3		100	300/75/30/30/40	5.3/1.2/1.95/3.18/1.95	
OR-2207H	510	15	4.3	79.2		75	360/50/30/30/40	3.0/1.2/1.95/3.18/1.95	
OR-2115H	427	16	4.0	79.2		15	400/40/30/30/40	3.2/1.2/1.95/3.18/1.95	
OR-2211H	566	17	3.7	78.5		50	360/50/30/30/40	3.1/1.2/1.95/3.18/2.00	
OR-2219H	584	18	3.3	78.0		NA	360/50/30/30/40	3.0/1.2/1.95/3.18/2.00	
OR-2207H	616	19	3.0	77.3		75	360/50/30/30/40	3.0/1.2/1.95/3.18/1.95	
OR-2219H	484	6	4.6	79.3		NA	360/50/30/30/40	3.0/1.2/1.95/3.18/2.00	
						OF-2 (Cell 2)[(4)]			
A-611[d]	4450	A-1-1	e	f	IRC-72	15	360/50/35/30/35	3.0/1.1/1.7/>3.18/1.7	1150
A-601[d]	4440	-2	e	f		75	360/50/35/30/35	3.0/1.1/1.7/>3.18/1.7	
A-611[d]	2530	-3	e	f		15	360/50/35/30/35	3.0/1.1/1.7/>3.18/1.7	
A-611[d]	2530	-4	e	f		15	360/50/35/30/35	3.0/1.1/1.7/>3.18/1.7	
A-601[d]	1980	-5	e	f		75	360/50/35/30/35	3.0/1.1/1.7/>3.18/1.7	
A-601[d]	1980	-6	e	f		75	360/50/35/30/35	3.0/1.1/1.7/>3.18/1.7	
A-611[d]	4450	A-2-1	e	f		15	360/50/35/30/35	3.0/1.1/1.7/>3.18/1.7	
A-611[d]	4450	-2	e	f		15	360/50/35/30/35	3.0/1.1/1.7/>3.18/1.7	
A-601[d]	2520	-3	e	f		75	360/50/35/50/35	3.0/1.1/1.7/>3.18/1.7	
A-601[d]	2520	-4	e	f		75	360/50/35/50/35	3.0/1.1/1.7/>3.18/1.7	
A-611[d]	1980	-5	e	f		15	360/50/35/50/35	3.0/1.1/1.7/>3.18/1.7	
A-601[d]	1980	-6	e	f		75	360/50/35/50/35	3.0/1.1/1.7/>3.18/1.7	

Table 3. (Continued)

Fissile particle batch No.	Number of particles irradiated	Sample identification	Fast fluence E > 0.18 MeV (n/cm^2)	Burnup (% FIMA)	Resin	Conversion[a] (%)	Design[b] A/B/C/D/E (μm)	Density[b] A/B/C/D/E (g/cm^3)	Maximum fuel[c] temperature (°C)
OR-2329H	1920	A-3-2	e	f	IRC-72	0	375/20/35/30/35	3.2/<1.3/1.95/>3.18/2.0	1150
OR-2329H	1920	A-3-4	e	f		0	375/20/35/30/35	3.2/<1.3/1.95/>3.18/2.0	
OR-2322H	1080	A-3-5	e	f		15	360/50/35/30/35	3.1/<1.3/1.95/>3.18/2.0	
OR-2211H	1100	A-3-6	e	f		50	375/50/35/30/35	3.2/<1.3/1.95/>3.18/2.0	
OR-2208H	1040	A-3-7	e	f		100	360/50/35/30/35	3.0/<1.3/1.95/>3.18/2.0	
OR-2322H	850	A-3-9	e	f		15	375/50/35/30/35	3.2/<1.3/1.95/>3.18/2.0	
OR-2329H	850	A-3-10	e	f		0	375/20/35/30/35	3.2/<1.3/1.95/>3.18/2.0	
OR-2208H	820	A-3-11	e	f		100	360/50/35/30/35	3.0/<1.3/1.95/>3.18/2.0	
OR-2121H	1520	A-4-1	e	f	IRC-72	100	320/75/35/30/35	5.0/<1.3/1.95/>3.18/2.0	
OR-2332H	1940	A-4-2	e	f		0	375/50/35/30/35	3.2/<1.3/1.95/>3.18/2.0	
OR-2121H	1520	A-4-3	e	f		100	320/75/35/30/35	5.0/<1.3/1.95/>3.18/2.0	
OR-2332H	1940	A-4-4	e	f		0	375/50/35/30/35	3.2/<1.3/1.95/>3.18/2.0	
OR-2218H	960	A-4-5	e	f		0	360/50/35/30/35	3.7/<1.3/1.95/>3.18/2.0	
OR-2320H	1100	A-4-6	e	f		25	375/50/35/30/35	3.2/<1.3/1.95/>3.18/2.0	
OR-2207H	1080	A-4-7	e	f		75	360/50/35/30/35	3.0/<1.3/1.95/>3.18/2.0	
OR-2218H	750	A-4-9	e	f		0	360/50/35/30/35	3.7/<1.3/1.95/>3.18/2.0	
OR-2332H	860	A-4-10	e	f		0	375/50/35/30/35	3.2/<1.3/1.95/>3.18/2.0	
OR-2207H	850	A-4-11	e	f		75	360/50/35/30/35	3.0/<1.3/1.95/>3.18/2.0	
A-601[d]	1520	B-1-1	e	f	IRC-72	75	360/50/35/30/35	3.0/1.1/1.8/>3.18/1.8	1350
A-601[d]	1520	B-1-2	e	f		75			
A-601[d]	1290	B-1-3	e	f		75			
A-611[d]	1290	B-1-4	e	f		15			
A-611[d]	1290	B-1-5	e	f		15			
A-611[d]	1290	B-1-6	e	f		15			
A-601[d]	1520	B-2-1	e	f		75			
A-611[d]	1520	B-2-2	e	f		15			
A-611[d]	1290	B-2-3	e	f		15			
A-601[d]	1290	B-2-4	e	f		75			
A-601[d]	1290	B-2-5	e	f		75			
A-611[d]	1290	B-2-6	e	f		15			
OR-2329H	660	B-3-2	e	f	IRC-72	0	375/20/35/30/35	3.2/<1.3/1.95/>3.18/2.0	
OR-2322H	650	B-3-3	e	f		15	375/50/35/30/35	3.2/<1.3/1.95/>3.18/2.0	
OR-2211H	660	B-3-4	e	f		50	360/50/35/30/35	3.1/<1.3/1.95/>3.18/2.0	
OR-2208H	530	B-3-5	e	f		100	360/50/35/30/35	3.0/<1.3/1.95/>3.18/2.0	
OR-2329H	560	B-3-7	e	f		0	375/20/35/30/35	3.2/<1.3/1.95/>3.18/2.0	
OR-2322H	550	B-3-8	e	f		15	375/50/35/30/35	3.2/<1.3/1.95/>3.18/2.0	
OR-2218H	490	B-3-9	e	f		0	360/50/35/30/35	3.7/<1.3/1.95/>3.18/2.0	
OR-2208H	530	B-3-10	e	f		100	360/50/35/30/35	3.0/<1.3/1.95/>3.18.2.0	
OR-2329H	560	B-3-11	e	f		0	375/20/35/30/35	3.2/<1.3/1.95/>3.18/2.0	
OR-2322H	550	B-3-12	e	f		15	375/50/35/30/35	3.2/<1.3/1.95/>3.18/2.0	
OR-2332H	660	B-4-2	e	f	IRC-72	0	375/50/35/30/35	3.2/<1.3/1.95/>3.18/2.0	
OR-2218H	580	B-4-3	e	f		0	360/50/35/30/35	3.7/<1.3/1.95/>3.18/2.0	
OR-2320H	660	B-4-4	e	f		25	375/50/35/30/35	3.2/<1.3/1.95/>3.18/2.0	
OR-2207H	550	B-4-5	e	f		75	320/75/35/30/35	5.0/<1.3/1.95/>3.18/2.0	
OR-2121H	440	B-4-6	e	f		100	320/75/35/30/35	5.0/<1.3/1.95/>3.18/2.0	
OR-2332H	560	B-4-7	e	f		0	375/50/35/30/35	3.2/<1.3/1.95/>3.18/2.0	
OR-2218H	490	B-4-8	e	f		0	360/50/35/30/35	3.7/<1.3/1.95/>3.18/2.0	
OR-2320H	560	B-4-9	e	f		25	375/50/35/30/35	3.2/<1.3/1.95/>3.18/2.0	
OR-2207H	550	B-4-10	e	f		75	320/75/35/30/35	5.0/<1.3/1.95/>3.18/2.0	
OR-2332H	560	B-4-11	e	f		0	375/50/35/30/35	3.2/<1.3/1.95/>3.18/2.0	
					OF-2 (Cell 1)[(4)]				
A-601[d]	2500	C-1-1	e	f	IRC-72	75	360/50/35/30/35	3.1/1.1/1.8/>3.18/1.8	
A-601[d]	2500	C-1-2	e	f		75			
A-611[d]	2970	C-1-3	e	f		15			
A-601[d]	6790	C-1-4	e	f		75			
A-615[g]	2440	C-2-1	e	f		75			
A-601[d]	2500	C-2-2	e	f		75			
A-615[g]	2900	C-2-3	e	f		75			
A-615[g]	6648	C-2-4	e	f		75			
A-611[d]	2500	C-3-1	e	f		15			
A-611[d]	2500	C-3-2	e	f		15			
A-601[d]	2960	C-3-3	e	f		75			
A-611[d]	6800	C-3-4	e	f		15			
A-615[g]	2440	C-4-1	e	f		75			
A-611[d]	2500	C-4-2	e	f		15			
A-601[d]	2960	C-4-3	e	f		75			
A-601[d]	6790	C-4-4	e	f		75			

[a]Percent conversion = $\frac{2-x}{2} \cdot 100$, where x = atomic fraction of oxygen in kernel; e.g., $UCyO_{0.5}$ = 75% converted.

[b]A = kernel; B = buffer; C = IPyC; D = SiC; E = OPyC.

[c]Maximum fuel design temperature.

[d]12.7 cm (5 in.) diam frit.

[e]Peak fast fluence will be 8×10^{21} n/cm^2 at end of irradiation period.

[f]Peak burnup will be 80% FIMA at end of irradiation period.

[g]12.7 cm (5 in.) diam cone.

[1]F. J. Homan et al., *Irradiation Performance of HTGR Fuel Rods in HFIR Experiments HRB-4 and -5*, ORNL-5115, in publication.

[2]F. J. Homan et al., *Irradiation Performance of HTGR Fuel Rods in HFIR Experiment HRB-6*, ORNL-TM-5011 (December 1975).

[3]K. H. Valentine et al., *Irradiation Performance of HTGR Fuel Rods in HFIR Experiments HRB-7 and -8*, in preparation.

[4]*HTGR Base Technology Program Annu. Progr. Rep. Jan. 1, 1974 through June 30, 1975*, Sect. 6.5.3, in preparation.

Table 3a. Results of Irradiation Tests on Weak-Acid Resin-Derived Recycle Fuel

Sample identification	Remarks[a]
	HRB-5
1A, 1B, 1C	Extruded rods; carbonized in covered graphite tray; fine cracks in SiC observed; no amoeba.
3A, 3B	Slug-injected rods; carbonized in packed Al_2O_3. Matrix-particle interaction recognized as a potential problem with high pitch-coke yields. No amoeba. Kernel densification apparent.
3C, 3D	Slug-injected rods; carbonized in-block.
	HRB-4
1A, 1B, 1C	Extruded rods; carbonized in covered graphite tray; fine cracks in SiC observed; no amoeba.
3A, 3B	Slug-injected rods; carbonized in packed Al_2O_3. Attack of SiC coating by Pd and rare-earth fission products observed. Phase segregation in about 25% of the kernels. Metallographic results indicate not all particles were 95% converted.
3C, 3D	Slug-injected rods; carbonized in-block.
	HRB-6
1C4, 1C5	Loose particles in graphite tube; recovery of all particles not possible; majority failed.
1C6	Loose particles in graphite tube; tube broke during irradiation; particles lost.
	HRB-7
13	Slug-injected rod; no failures (Metallography); buffer consumed; slight attack of SiC by rare earths.
14	Slug-injected rod; ∿ 50% failed (Metallography); ILTI graphitized by rare earths on cold side.
15	Slug-injected rod; no failures (Metallography); buffer consumed; phase segregation in kernel; no evidence of rare earth in coatings.
16	Slug-injected rod; no failures (Metallography); unilateral movement of kernel through buffer; no evidence of rare earth in coatings.
	HRB-8
13	Slug-injected rod; no failures (Metallography); buffer consumed; slight attack of SiC by rare earths.
14	Slug-injected rod; all failed (Metallography); ILTI graphitized by rare earths on cold side.
15	Slug-injected rod; no failures (Metallography); buffer consumed; phase segregation in kernel; no evidence of rare earth in coatings.
16	Slug-injected rod; no failures (Metallography); kernel densification apparent; buffer intact; no evidence of rare earth in coatings.
	HRB-9
1, 3, 4, 5	Slug-injected rod; stereo-exam only. No broken particles on surface.
6	Slug-injected rod; ∿ 20% failed (Metallography); buffer in half of particles densified and breached; two-phase kernel; Slight accumulation of rare earths on cold side; no graphitization of ILTI; slight attack of SiC.
8	Slug-injected rod; no failures (Metallography); buffer consumed; phase segregation in kernel.
9	Slug-injected rod; no failures (Metallography); buffer intact; phase segregation in kernel; evidence of rare earth accumulation on cold side; no graphitization of ILTI; no attack of SiC
10	Warm-molded rod; no failures (Metallography); buffer intact; phase segregation in kernel; less evidence of rare earth accumulation in rod 9; no graphitization of ILTI; no attack of SiC.
11	Slug-injected rod; ∿ 75% failed (Metallography); accumulation of rare earth on cold side; graphitization of ILTI; no attack of SiC; two-phase kernel.
12	Slug-injected rod; no failures (Metallography); amoeba through buffer; rare earths retained in kernel; slight attack of SiC on hot side (2 μm).
13	Slug-injected rod; no failures (Metallography); buffer intact but densified around kernel; phase segregation in kernel; accumulation of rare earths on cold side; no graphitization of ILTI; no attack of SiC.
14	Slug-injected rod; ∿ 50% failed (Metallography); phase segregation in kernel; accumulation of rare earths on cold side; graphitization of ILTI; attack of SiC (∿ 5 μm).
15	Slug-injected rod; stereo-exam only; no failures.
16	Slug-injected rod; no failures (Metallography); buffer consumed; phase segregation in kernel.
17	Slug-injected rod; same remarks as for HRB-9, Rod 13 (50% converted).
18	Slug-injected rod; stereo-exam only; no broken particles.
19	Slug-injected rod; stereo-exam only; no broken particles.
	HRB-10
1	Slug-injected rod; not examined, due to reaction with thermocouple.
3	Slug-injected rod; stereo-exam only; no broken particles.
4, 5	Slug-injected rod; stereo-exam only; no broken particles.
6	Slug-injected rod; ∿ 30% failed (Metallography); accumulation of rare earths on cold side; graphitization of ILTI and buffer; attack of SiC with complete penetration.
8	Slug-injected rod; no failures (Metallography); buffer consumed; phase segregation in kernel.
9	Slug-injected rod; ∿ 8% failed (Metallography); phase segregation in kernel; accumulation of rare earths on cold side. slight graphitization of ILTI; no attack of SiC.
10	Warm-molded rod; no failures (Metallography); phase segregation in kernel; accumulation of rare earths on cold side; no graphitization of ILTI; slight attack of SiC.
11	Slug-injected rod; ∿ 18% failed (Metallography); two-phase kernel; accumulation of rare earths on cold side; graphitization of ILTI; attack of SiC (∿ 5 μm).
12	Slug-injected rod; ∿ 5% failed (Metallography); amoeba through buffer; rare earths retained in kernel; attack of SiC (slight to complete penetration).
13	Slug-injected rod; no failures (Metallography); same remarks as for HRB-9, Rod 13 (50% converted), except more evidence of rare-earth accumulation.
14	Slug-injected rod; ∿ 30% failures (Metallography); two-phase kernel, accumulation of rare earths on cold side; graphitization of ILTI; attack of SiC (complete penetration).

Table 3a. (Continued)

Sample identification	Remarks[a]
15	Slug-injected rod; no failures (Metallography); accumulation of rare earths on cold side; slight graphitization of ILTI; no attack of SiC; phase segregation in kernel.
16, 17	Slug-injected rod; stereo-exam only; no broken particles.
18	Slug-injected rod; ∿ 40% failed (Metallography); same remarks as for HRB-10, Rod 6.
19	Slug-injected rod; no failures (Metallography); phase segregation in kernel; no accumulation of rare earths; no graphitization of ILTI; no attack of SiC.
	OF-2 (Cell 2)
A-1-1, -2, -3, -4, -5, -6 A-2-1, -2, -3, -4, -5, -6	All slug-injected rods; initial R/B values for $^{85m}Kr = 7.5 \times 10^{-6}$; After 4200 hr (∿ 1/2 irradiation time) R/B $^{85m}Kr = 1 \times 10^{-5}$. Postirradiation examination scheduled to begin in September 1976.
A-3-2, -4, -5, -6, -7, -9, -10, -11 A-4-1, -2, -3, -4, -5, -6, -7, -9, -10, -11 B-1-1, -2, -3, -4, -5, -6, B-2-1, -2, -3, -4, -5, -6 B-3-2, -3, -4, -5, -7, -8, -9, -10, -11, -12 B-4-2, -3, -4, -5, -6, -7, -8, -9, -10, -11	All slug-injected rods; initial R/B values for $^{85m}Kr = 7.5 \times 10^{-6}$. After 4200 hr (∿ 1/2 irradiation time) R/B $^{85m}Kr = 1 \times 10^{-5}$. Postirradiation examination scheduled to begin in September 1976.
	OF-2 (Cell 1)
C-1-1, -2, -3, -4 C-2-1, -2, -3, -4 C-3-1, -2, -3, -4 C-4-1, -2, -3, -4	All fuel rods fabricated by slug-injection process. Initial ^{85m}Kr R/B values = < 2×10^{-5}; After 4200 hr irradiation (∿ 1/2 full scheduled term) ^{85m}Kr R/B value = 7×10^{-5}. Postirradiation examination scheduled to begin in September 1976.

[a]References to "% failed particles" are based on failures observed in metallographic sections, and therefore are not statistically significant since normally < 20 fissile particles are exposed in a random plane-of-polish. These results are, however, indicators of relative performance.

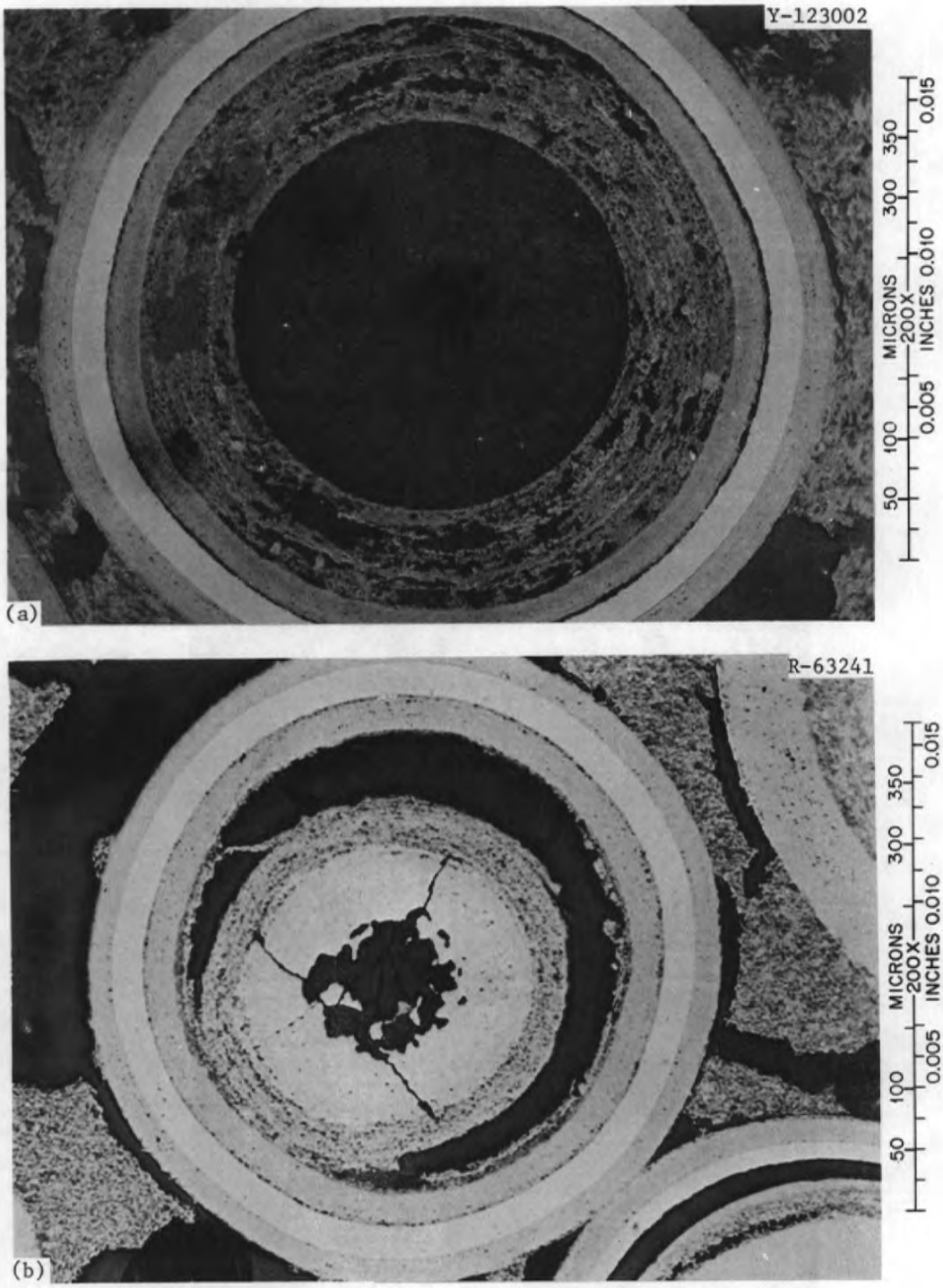

Fig. 8. Weak-Acid Resin Particles Used in Slug-Injected Fuel Rods for Irradiation Testing. (a) Unirradiated. (b) Irradiated in HRB-5, rod 3B. Typical of particles in the cross section of the fuel rod. Time-averaged temperatures ranged from 1150 to 1400°C with peak temperature of 1525°C.

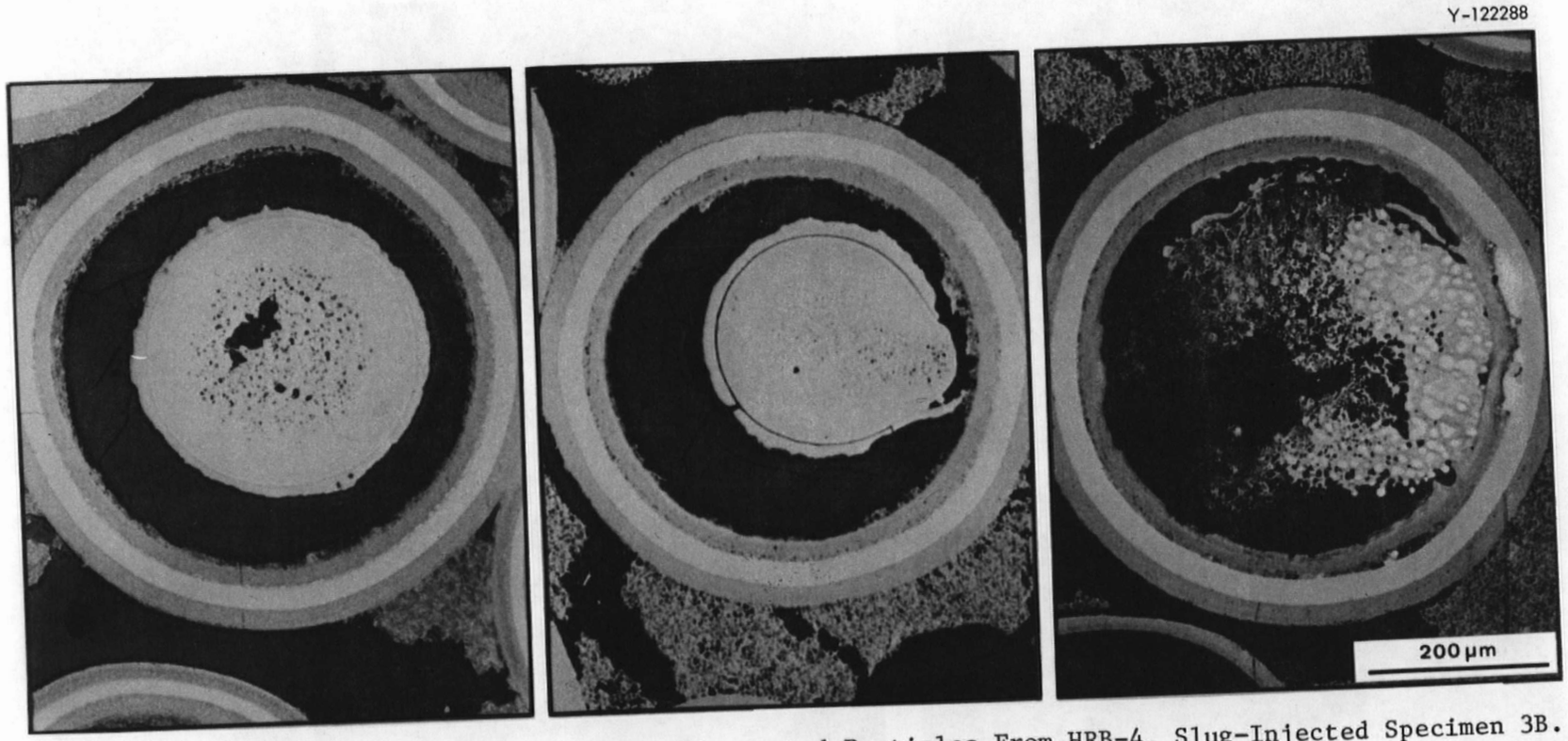

Fig. 9. Appearance of Weak-Acid Resin Fissile Coated Particles From HRB-4, Slug-Injected Specimen 3B.

R-70001

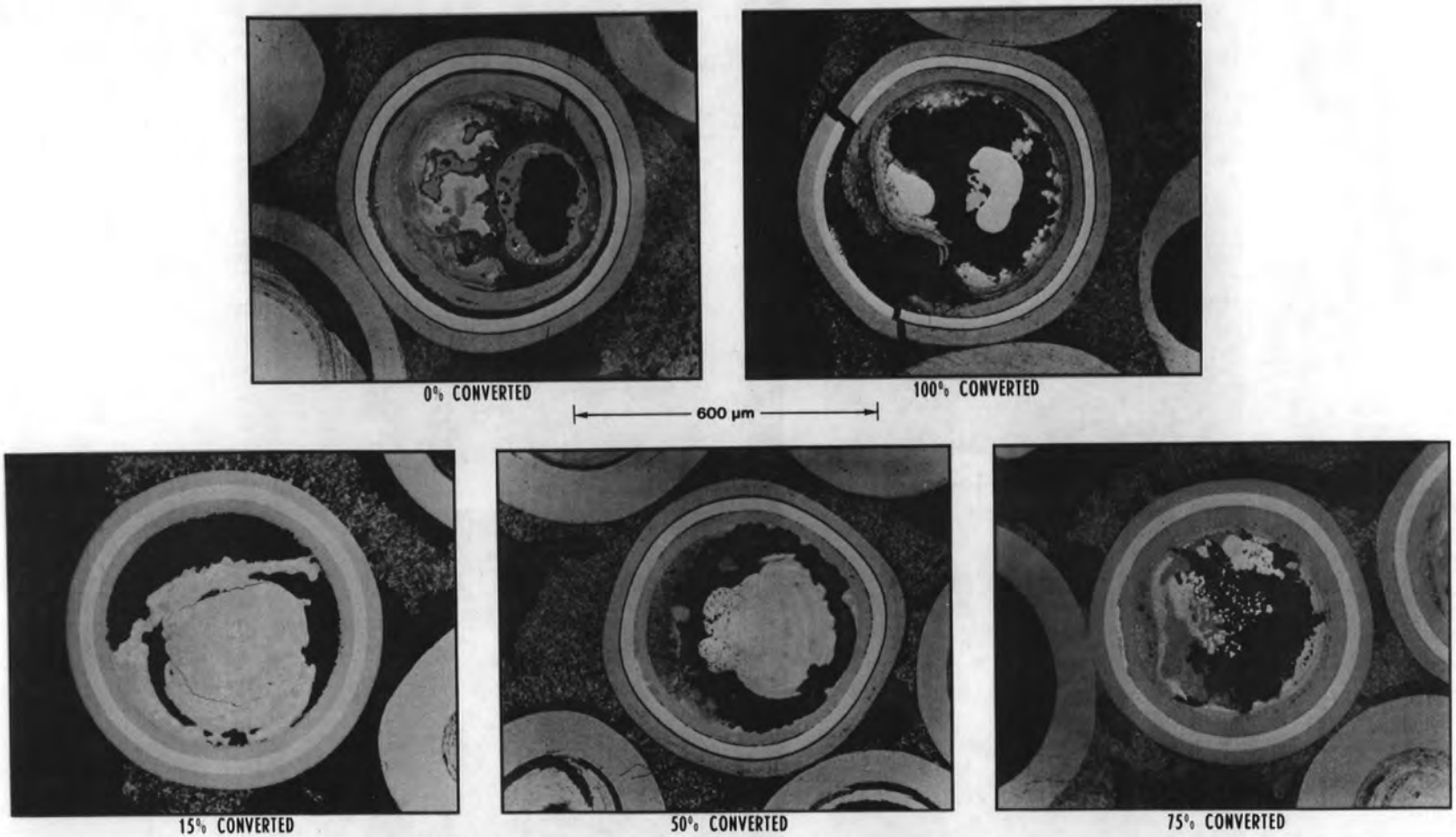

Fig. 10. Relative Performance of Weak-Acid Derived Kernels Converted Within the Range of UO_2 (0% Converted) to UC_2 (100% Converted). Irradiated at a maximum fuel temperature of 1500°C to a burnup of 80% FIMA. Fast fluence ranged from 4.3 to 5.0×10^{21} n/cm^2 (E > 0.18 MeV). The two particles at the top of the figure are from the peripheral regions of fuel rods and operated at less than peak rod temperatures but demonstrate performance limitations in steep thermal gradient (>800°C/cm) conditions. The hot side of the particles is on the right.

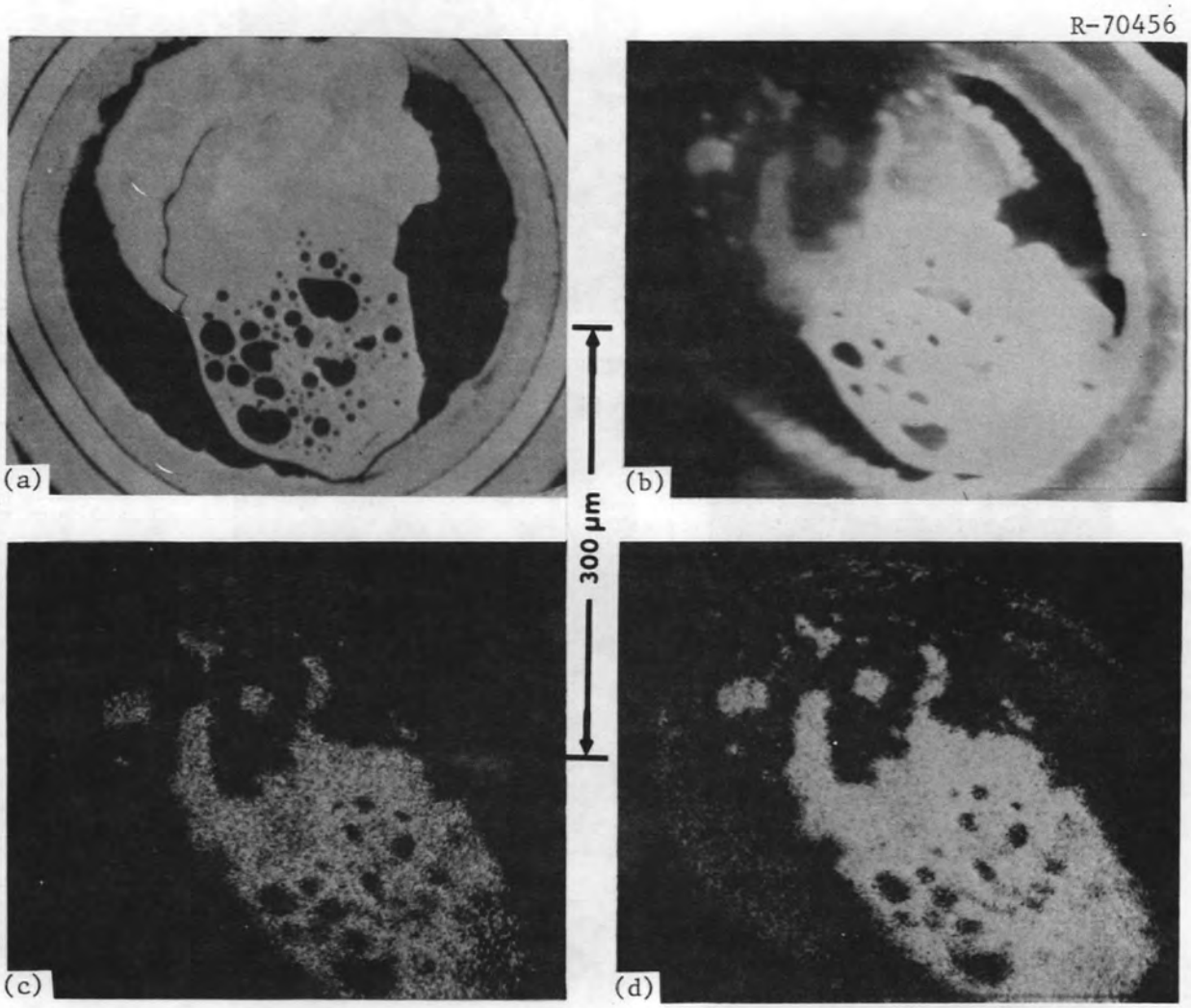

Fig. 11. Distribution of Uranium and Rare-Earth Fission Products (Typified by Nd X-Ray Display) in a 15% Converted Weak-Acid Resin-Derived Particle. There is no indication that the Nd penetrated the inner pyrocarbon layer. (a) Optical micrograph. (b) Backscattered electron image. (c) U M_β. (d) Nd L_α.

Y-12086

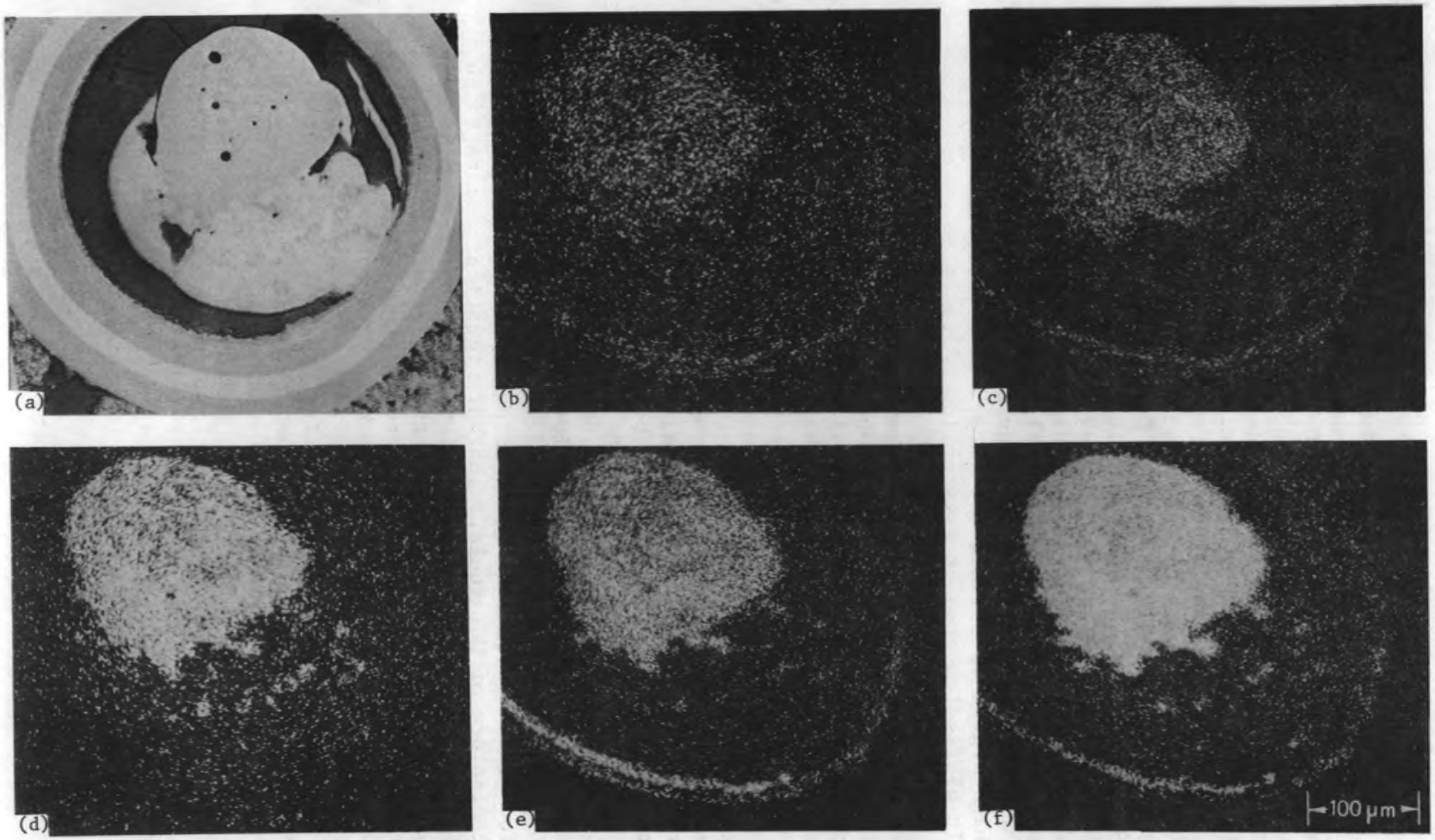

Fig. 12. Distribution of Uranium and Rare-Earth Fission Products in a Triso-Coated 15% Converted Weak-Acid Resin Particle Irradiated in HRB-8. (a) Optical micrograph. (b) La L_α. (c) Pr L_α. (d) U M_β. (e) Ce L_α. (f) Nd L_α.

4. There is considerable fission product attack of the SiC coatings by rare-earth fission products La, Ce, Pr, and Nd in WAR UC_2 fuels. This same type of attack has been observed in dense UC_2 fuels irradiated in HRB capsules under accelerated conditions, and also in the Peach Bottom Reactor under real-time conditions. The presence of UO_2 reduces the amount of fission product attack of the SiC layer, apparently due to the formation of stable rare-earth oxides, which are retained in the kernel. Optical metallography and shielded microprobe displays of nominally 95% UC_2 fuel irradiated in the HRB-4 capsule are shown in Fig. 13. A similar display of reference fresh fissile fuel (UC_2) irradiated under real-time conditions in the Peach Bottom Reactor is shown in Fig. 14. (Note that the UC_2 shown in Fig. 14 has been irradiated to less than 20% full burnup and to less than 20% of the fast neutron exposure expected for the LHTGR.[14]) The similarity of fission product deposition in WAR UC_2 and dense UC_2 fuel irradiated in HRB-7 is shown in Fig. 15. The polarized-light portion of this figure reveals regions having a high degree of optical activity, which indicates graphitization as a result of fission product interaction.

5. There is a considerable temperature gradient effect on the fission product attack. Under high-temperature gradients, the fission products are concentrated on the cold side of the particle, and failure of the SiC layer is likely, as shown on the left side of Fig. 16. Under less severe temperature gradients, the fission products are less concentrated and do less damage. The particle shown on the right side of Fig. 16 was operated at the center of the same fuel rod. The temperature gradient is zero at the center of the rod, and even though the operating temperature was higher at this position, less damage was done to the coatings by the fission products. The bottom portion of Fig. 16 (in polarized light) shows the light regions where fission products are present. The temperature gradient of 1000°C/cm is about 30% higher than the maximum temperature gradient for an LHTGR (Table 1).

Fission product attack of the coatings appears to be the limiting performance feature of UC_2 fuels. Thermal migration appears to be limiting for UO_2. Intermediate stoichiometries appear to perform well compared with these extremes. In the HRB-7 through -10 series of experiments, WAR fissile fuels with conversion levels of 0, 15, 50, 75, and 100% were tested. These WAR kernels were coated with reference Triso coatings and were fabricated into fuel rods using the slug-injection technique. As indicated earlier, the WAR UO_2 kernel has migrated up the temperature gradient, and the WAR UC_2 particle has failed due to fission product attack of the SiC layer. Figure 17 shows an optical photomicrograph of a WAR UC_2 particle irradiated in HRB-8. Also shown are electron microprobe displays for the rare-earth fission products La, Pr, Ce, and Nd. The graphitization of the inner pyrolytic carbon coating and failure of the SiC in the regions occupied by the fission products indicates failure due to chemical interaction.

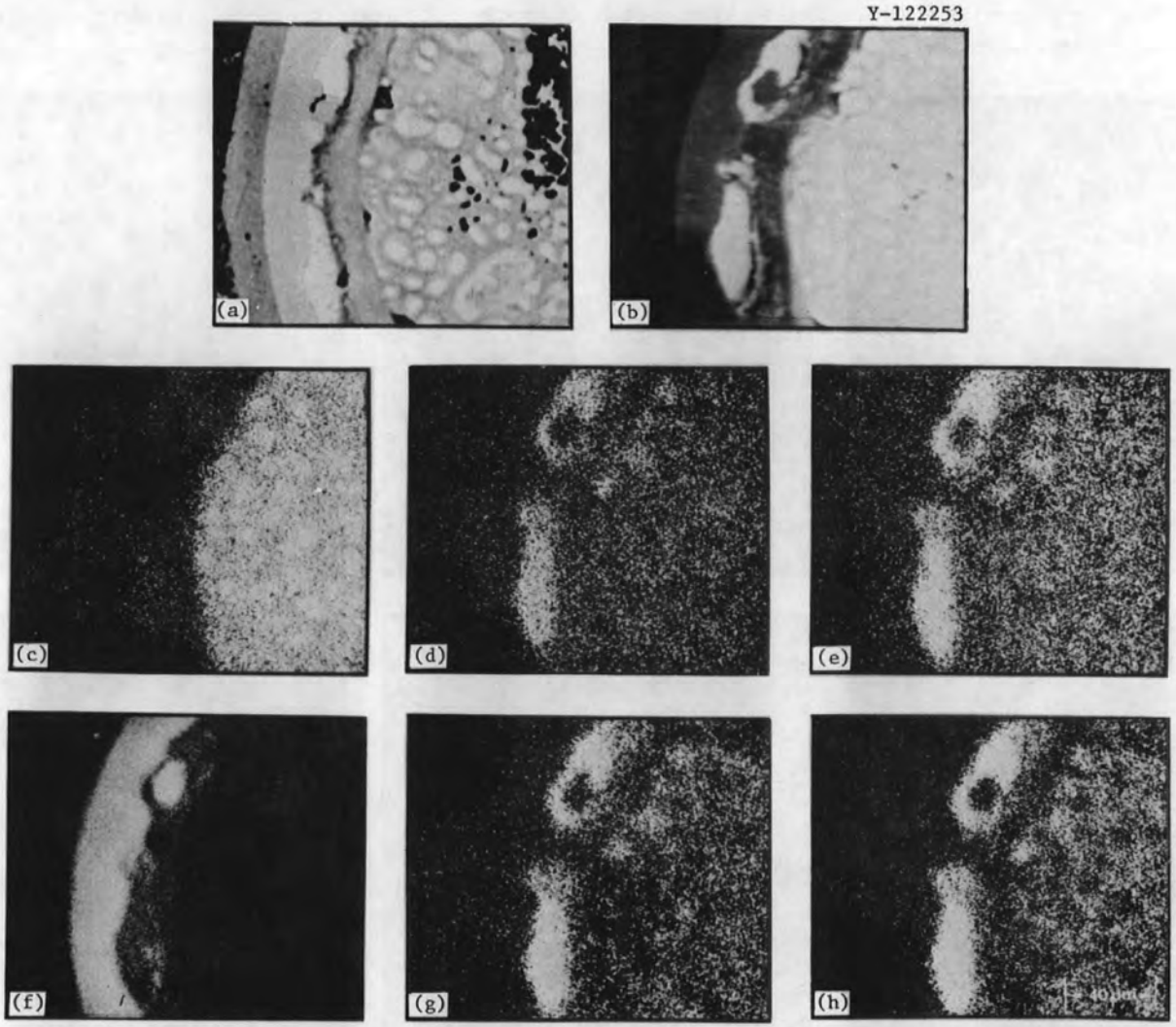

Fig. 13. Weak-Acid Resin Particle From Fuel Rod 3B, Irradiation Capsule HRB-4. (a) Optical photograph. (b) Backscattered electron. (c) U M_α. (d) La L_α. (e) Pr L_α. (f) Si L_α. (g) Ce L_α. (h) Nd L_α.

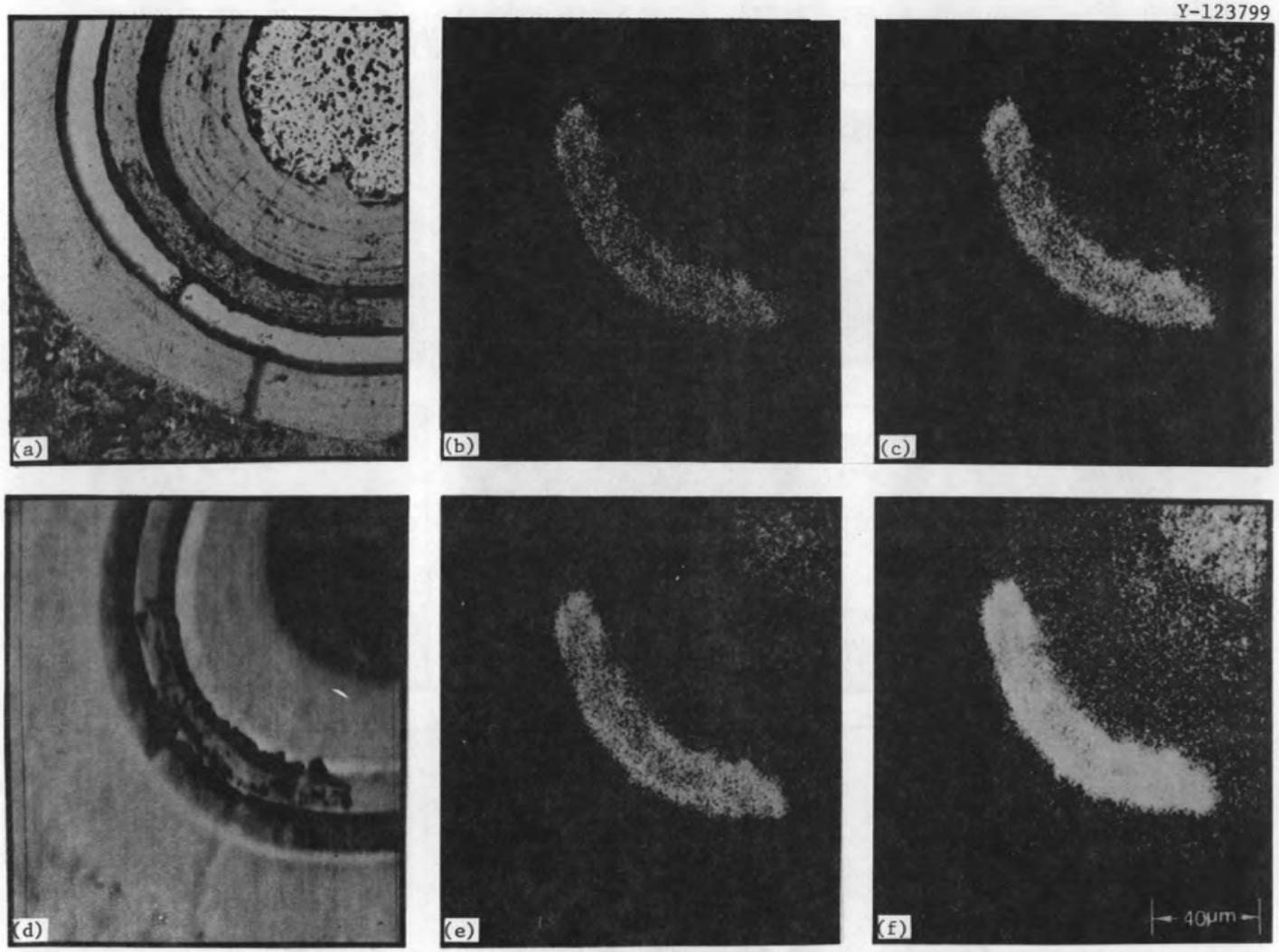

Fig. 14. Rare-Earth Fission Products Found on Cold Side of Triso-Coated Dense UC_2 Kernel from RTE-4. (a) Optical micrograph. (b) La L_α. (c) Pr L_α. (d) Back-scattered electrons. (e) Ce L_α. (f) Nd L_α.

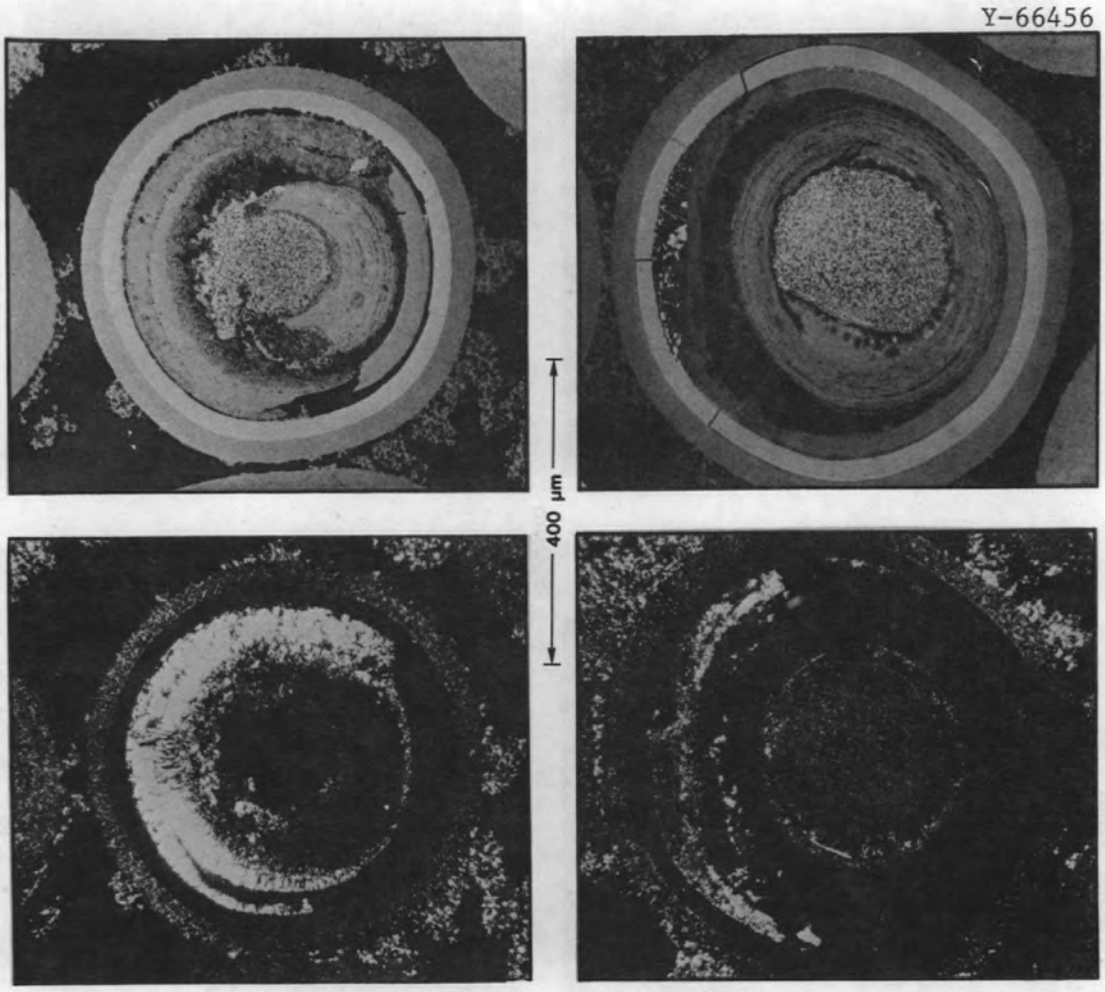

Fig. 15. Relative Performance of Dense UC_2 and WAR UC_2 in Irradiation Capsule HRB-7. Top: Bright field. Bottom: Polarized light. Left: UC_2 (VSM). Right: WAR — 100% reduced.

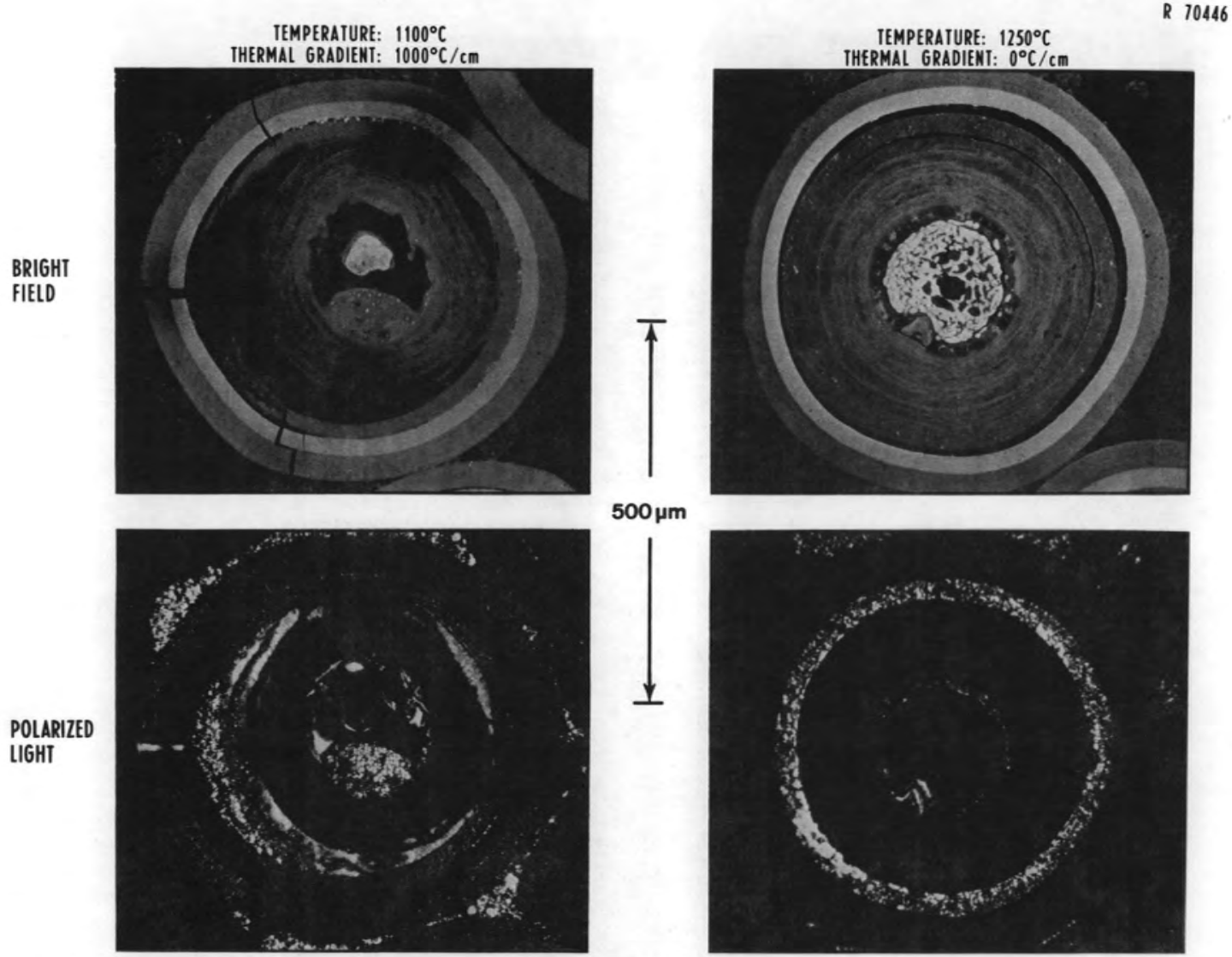

Fig. 16. Effect of Thermal Gradient on Distribution of Rare-Earth Fission Products in a Triso-Coated 100% Converted WAR UC_2 Kernel.

Y-127988

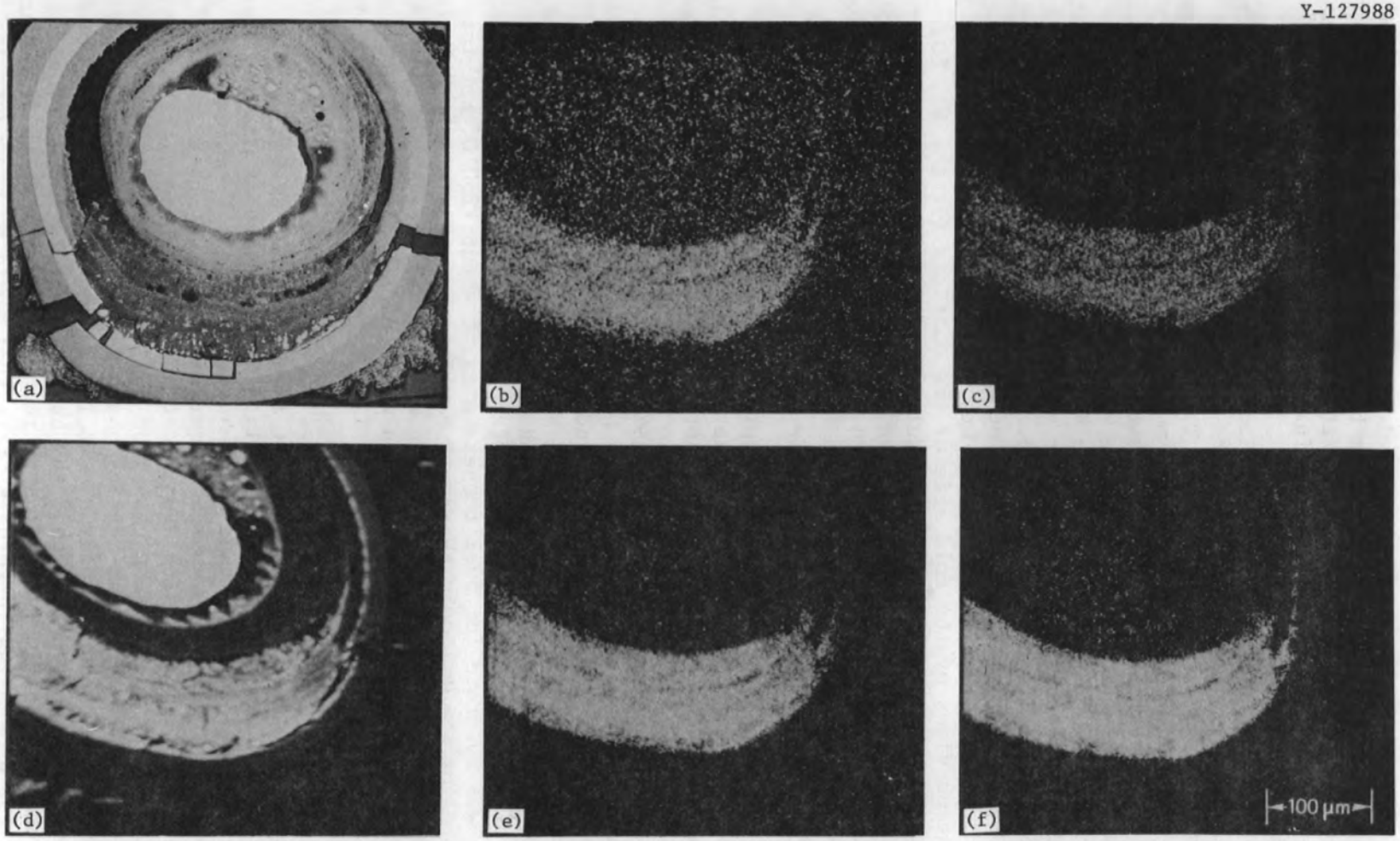

Fig. 17. Distribution of Rare-Earth Fission Products in a Triso-Coated 100% Reduced Weak-Acid Resin Particle Irradiated in HRB-8. (a) Optical micrograph. (b) La L_α. (c) Pr L_α. (d) Back-scattered electron image. (e) Ce L_α. (f) Nd L_α.

The thermodynamic arguments associated with kernel stoichiometry are discussed in ref. 1. Calculations have been made of the amount of UO_2 necessary to keep all the rare-earth fission products in the form of oxides in WAR fuels irradiated to full burnup [about 75% fissions per initial heavy-metal atom (FIMA)]. The irradiation results from HRB-7 through -10 support the conclusions reached in these calculations. UO_2 fuel (Fig. 18) retains all the rare-earth fission products in the kernel in the form of stable oxides. The 15% converted WAR fuel shown in Figs. 11 and 12 have also retained most of the rare-earth fission products (~93%) within the kernel. As the amount of UC_2 in the kernel is increased, the capacity to hold the rare-earth fission products within the kernel is reduced, as shown in Figs. 19 and 20. The slight accumulation of neodymium at the inner surface of the SiC layer in 50% converted fuel is shown in Fig. 19. Most of the neodymium, however, has been retained in the kernel. The neodymium display in this figure is also representative of La, Pr, and Ce. Figure 20 shows higher magnification views of the cold side of the coatings for the 15, 50, and 75% converted fuels. Slight accumulations of fission products, believed to be rare earths, can be seen at the SiC-inner LTI interface for particles with 50 and 75% converted kernels. The amount of fission product accumulation increased with an increase in the percentage of UC_2 present.

The question of optimum kernel stoichiometry for WAR fuels has not yet been answered. Experiments that have been designed to establish the optimum UO_2 content are now in-reactor. Based on the results from HRB-7 through -10 and the thermodynamic calculations,[1] it is anticipated that the optimum value will be about 35% conversion, with a range of ±20% permitted. The arguments against high UC_2 content are clear. Some problems have also been encountered with high UO_2 content, in addition to the amoeba already noted. While no fission product attack of the SiC layer was noted with the WAR UO_2 fuel, there was some evidence of oxidation of the inner surface of the SiC layer. The amount of attack was moderate for fuel temperatures of about 1250°C, but for temperatures of about 1500°C there was complete penetration of the SiC. Examples of the oxidation of the SiC in WAR UO_2 fuel are shown in Fig. 21. Fuel of this same composition was irradiated in capsule HRB-9 at a design center line temperature of 1250°C, and very slight oxidation was noted.

From the processing standpoint, it is desirable to maximize the UO_2 content in the two-phase WAR kernels. Considerable effort has therefore been expended to understand the behavior of the 15% converted fuel from HRB-7 through -10, which is currently thought to be the lower limit for the conversion specification.[1] Phase segregation shown in Figs. 11 and 12 is apparent both from optical examination and from microprobe work. The uranium-bearing phase is retained within the outer boundary of the buffer layer. It is apparent from the work done to date on 15% converted fuel that the buffer layer is largely incorporated into the kernel. According to the current definition of failure, developed for dense fissile kernels, this fuel would be unacceptable.

Y-129593

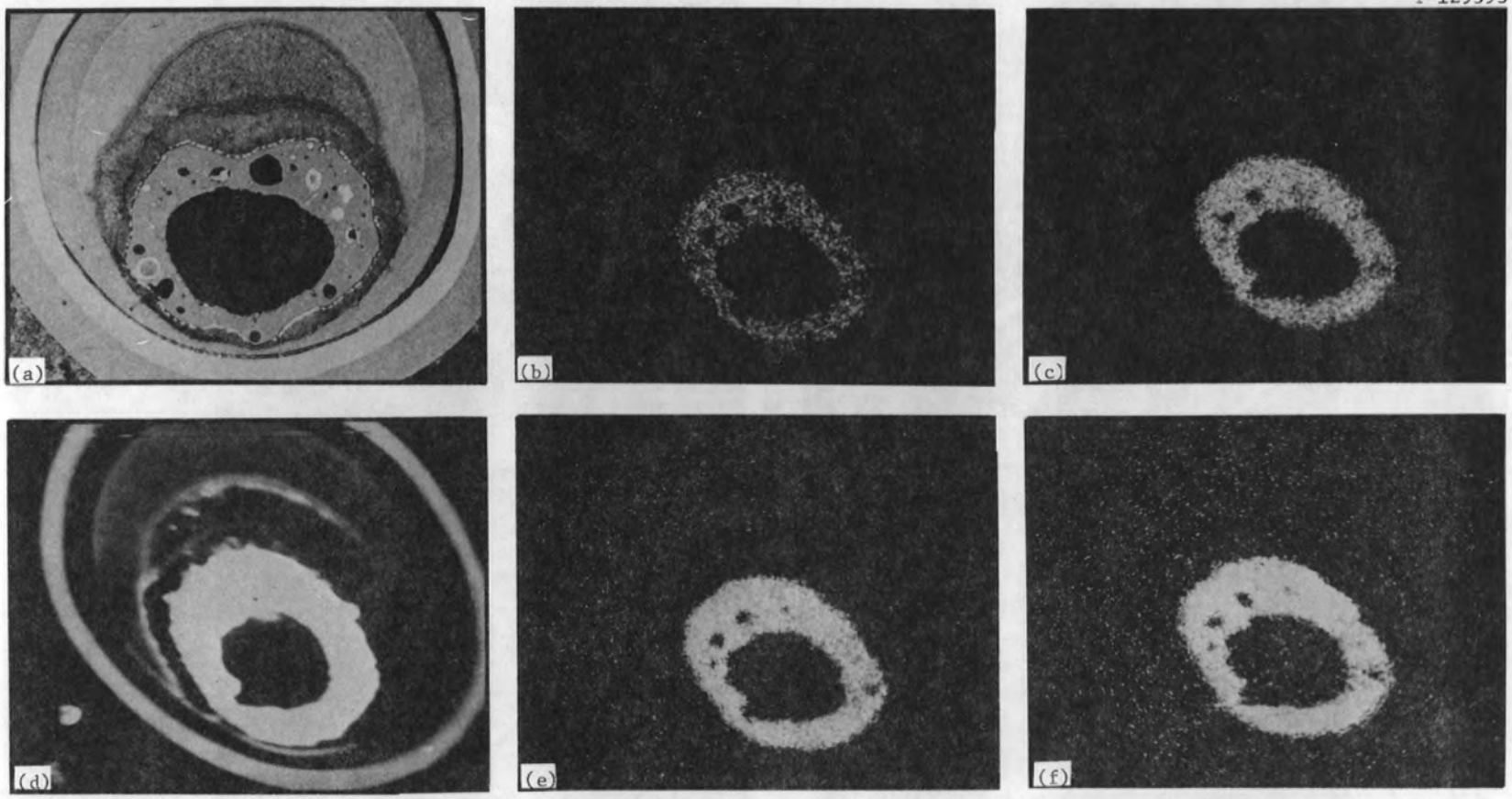

Fig. 18. Retention of Rare-Earth Fission Products in the Kernel of a Sol-Gel UO_2 Triso-Coated Particle Irradiated in HRB-8. 180×. (a) Optical micrograph. (b) La L_α. (c) Pr L_α. (d) Sample current image. (e) Ce L_α. (f) Nd L_α.

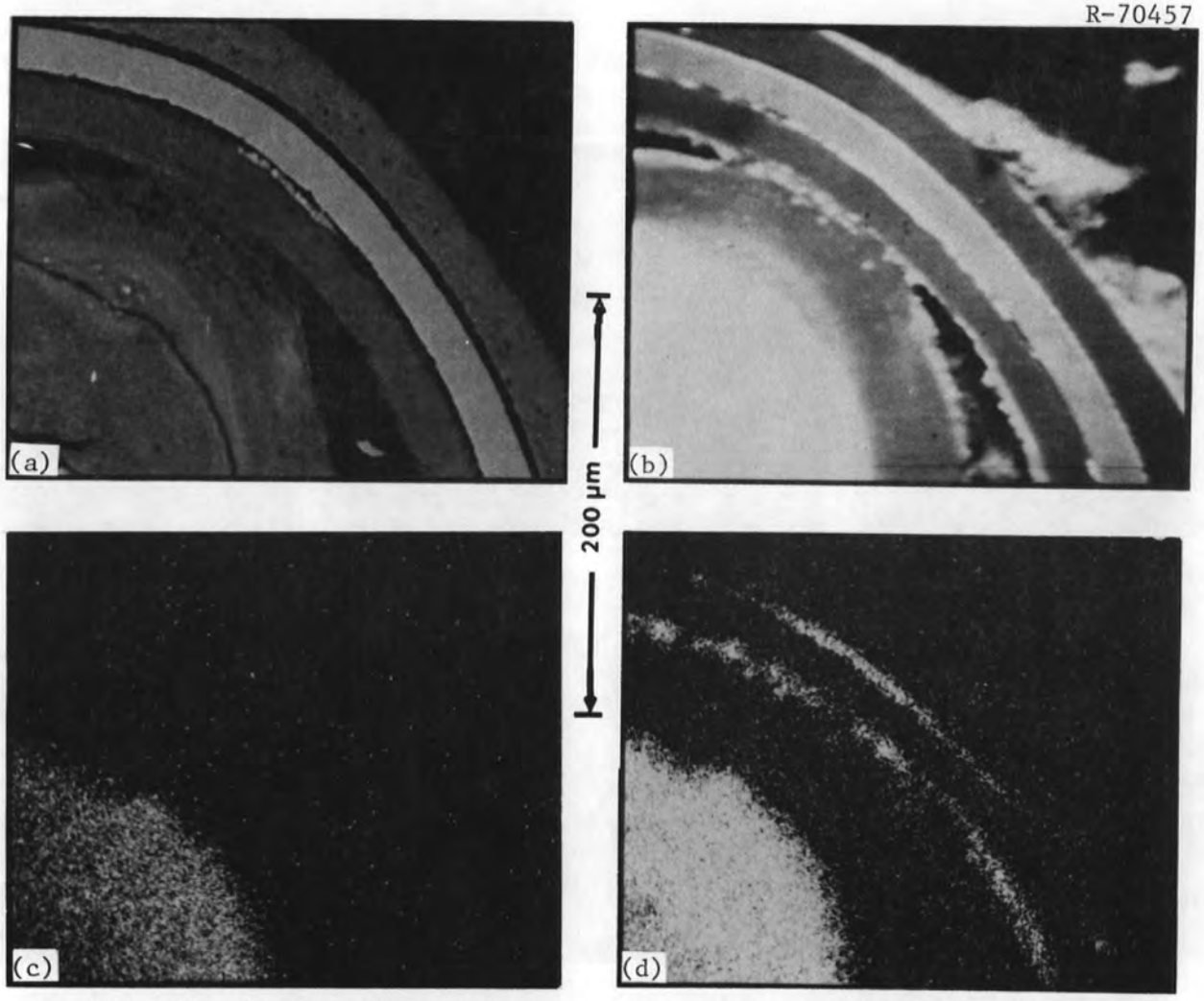

Fig. 19. Distribution of Uranium and Rare-Earth Fission Products (Typified by Nd X-Ray Display) in a 50% Converted Weak-Acid-Derived Particle. Note that Nd is present at the inner surface of the SiC coating. (a) Optical micrograph. (b) Backscattered electron image. (c) U M_β. (d) Nd L_α.

R-70447

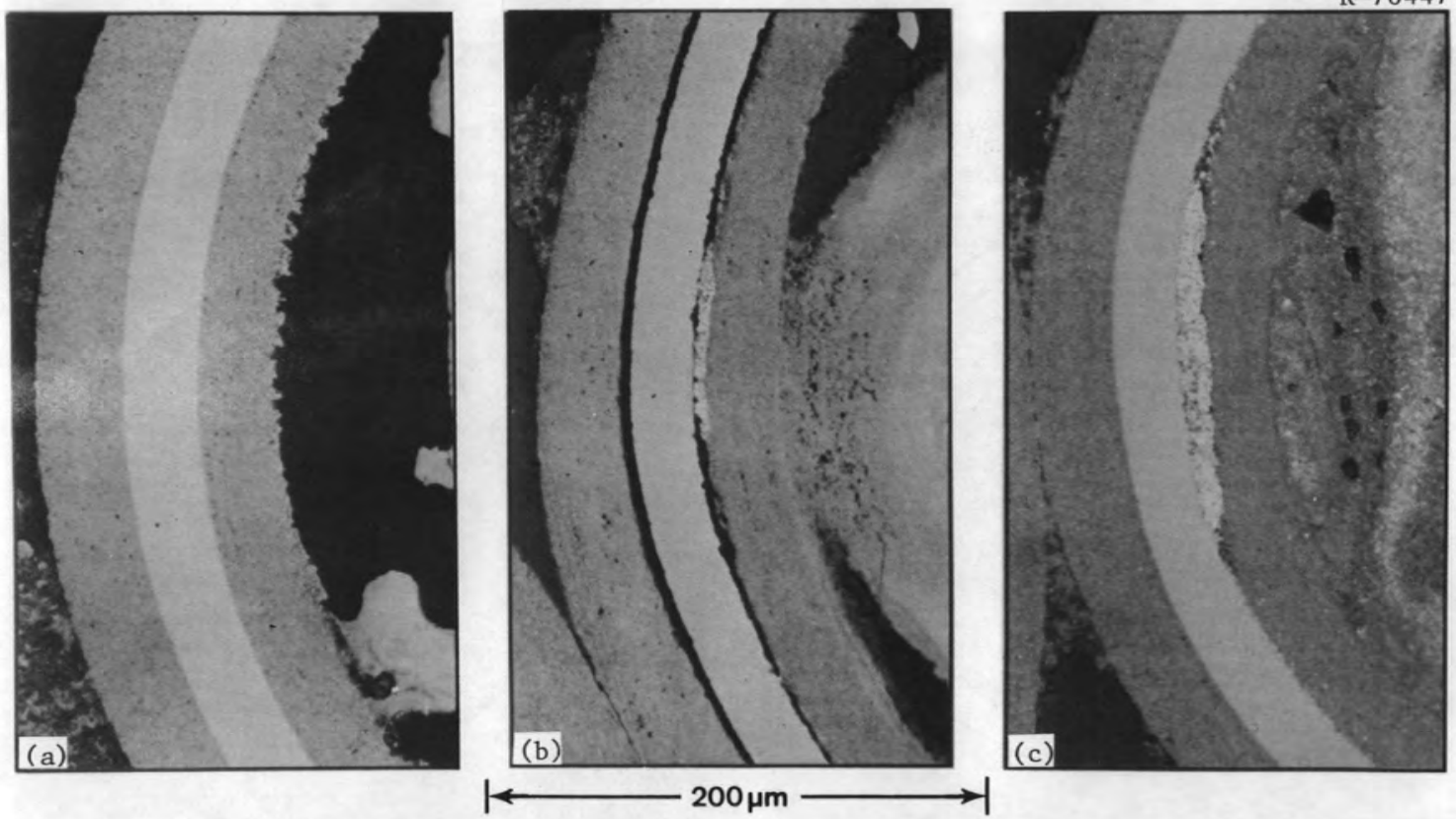

Fig. 20. Accumulation of Rare-Earth Fission Products at the SiC-Inner PyC Interface on the Cold Side of Triso-Coated Weak-Acid-Derived Kernels. Note the absence of fission products in the coatings of the 15% converted kernel. (a) 15% converted. (b) 50% converted. (c) 75% converted.

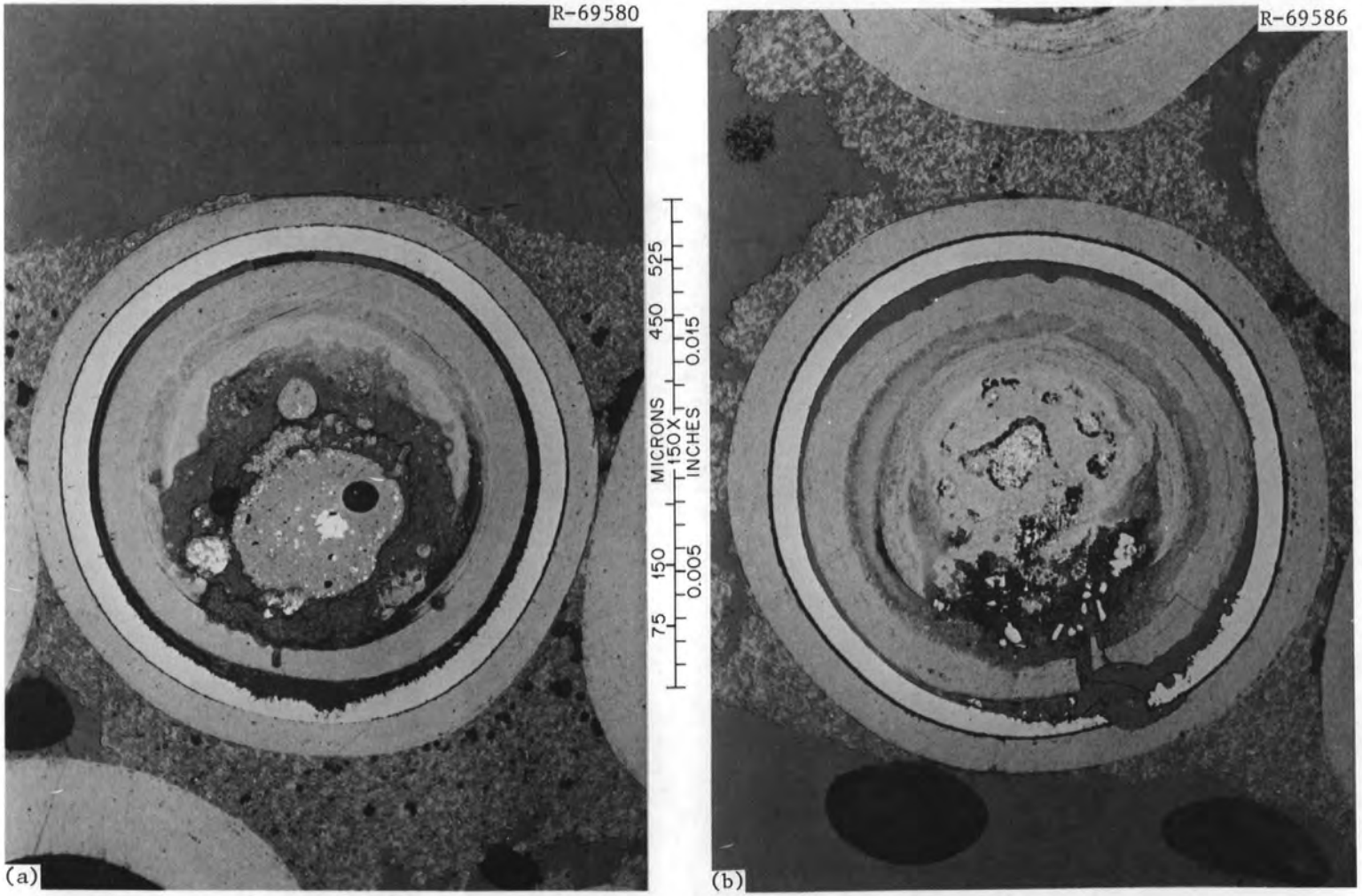

Fig. 21. Oxidation of the SiC Layer in WAR UO_2 Fuel Irradiated in HRB-10. (a) Irradiated on the surface of the fuel rod at about 1200°C. (b) Irradiated at the center of the fuel rod at about 1500°C.

However, it is currently believed that this definition of failure is not appropriate for WAR fuels. For fissile particles containing dense oxide kernels that are migrating up the temperature gradient, migration through the buffer means that the integrity of the pressure vessel has been compromised. Thus, failure is defined as migration through the buffer layer. However, for fissile particles containing WAR UO_2-UC_2 kernels with more than the 15% carbide phase, temperature gradient dependent migration of the kernel has not been observed. The incorporation of the buffer layer into the kernel does not appear to influence the integrity of the outer coating layers. Irradiation testing is under way to prove statistically that the 15% converted WAR fuel meets the performance criteria for fissile particles. Quantitative electron microprobe results have shown that the 15% converted kernels retain all but about 7.5% of the rare-earth fission products that form during irradiation. Quantitative work is under way for kernels of 50 and 75% conversion, but it is certain that these fuels will release more fission products than the 15% converted fuel, based on the optical comparisons that have already been made.

PERFORMANCE OF COATED PARTICLES AND FUEL RODS

Of the five failure mechanisms for coated particle fuels listed in the Introduction, the first two have been described thoroughly in the previous sections of this report. The remaining three mechanisms will be described in this section.

Pressure vessel failure is only slightly dependent on the kernel type. As noted earlier, the WAR-derived kernels are considerably more porous than dense oxides or carbides and tend to shrink appreciably during irradiation. Both of these effects contribute to higher fission gas release at low burnup. High porosity fractions provide an easy route for fission gas release, and the kernel shrinkage and high porosity content contribute to higher kernel operating temperatures than would be experienced by dense kernels operating at the same power level. High operating temperatures drive more fission gas out of the kernel matrix. Pressure vessel failure is not considered to be a serious problem for recycle fissile fuel, since thicker SiC coatings that will withstand the higher fission gas release can be specified. An example of pressure vessel failure is shown in Fig. 22.

Matrix-particle interaction occurs when a strong bond forms between the matrix and the outer coating layer. Both matrix and coatings shrink during irradiation, causing the outer coating to fracture or separate. An example is shown in Fig. 23. The most exaggerated matrix-particle interaction seen was in the HRB-4 and -5 experiment[12] where the fuel rods were carbonized in a graphite tube to simulate in-block carbonization. No interaction was observed in fuel rods carbonized in beds of packed alumina; presumably because the volatile hydrocarbons are more easily removed.

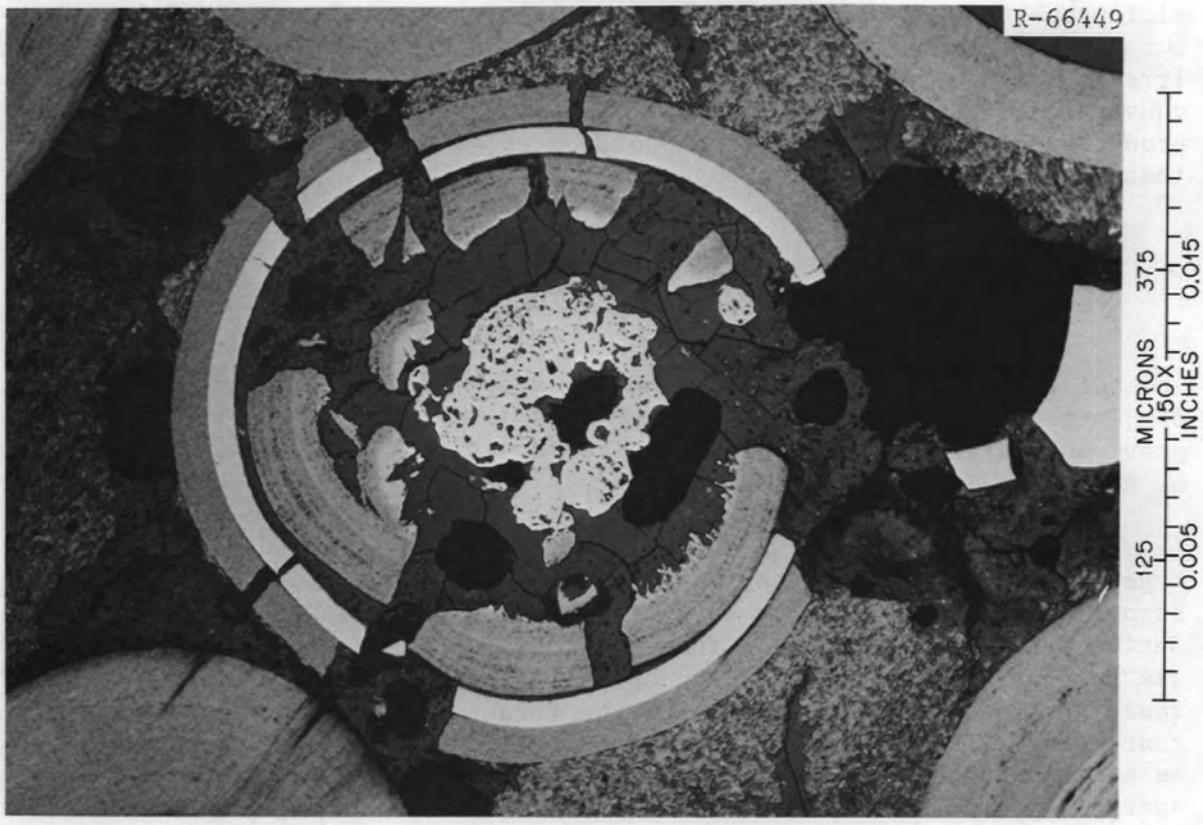

Fig. 22. Pressure Vessel Failure in HRB-8, Specimen 5 ($^{233}UO_2$).

Y-119989

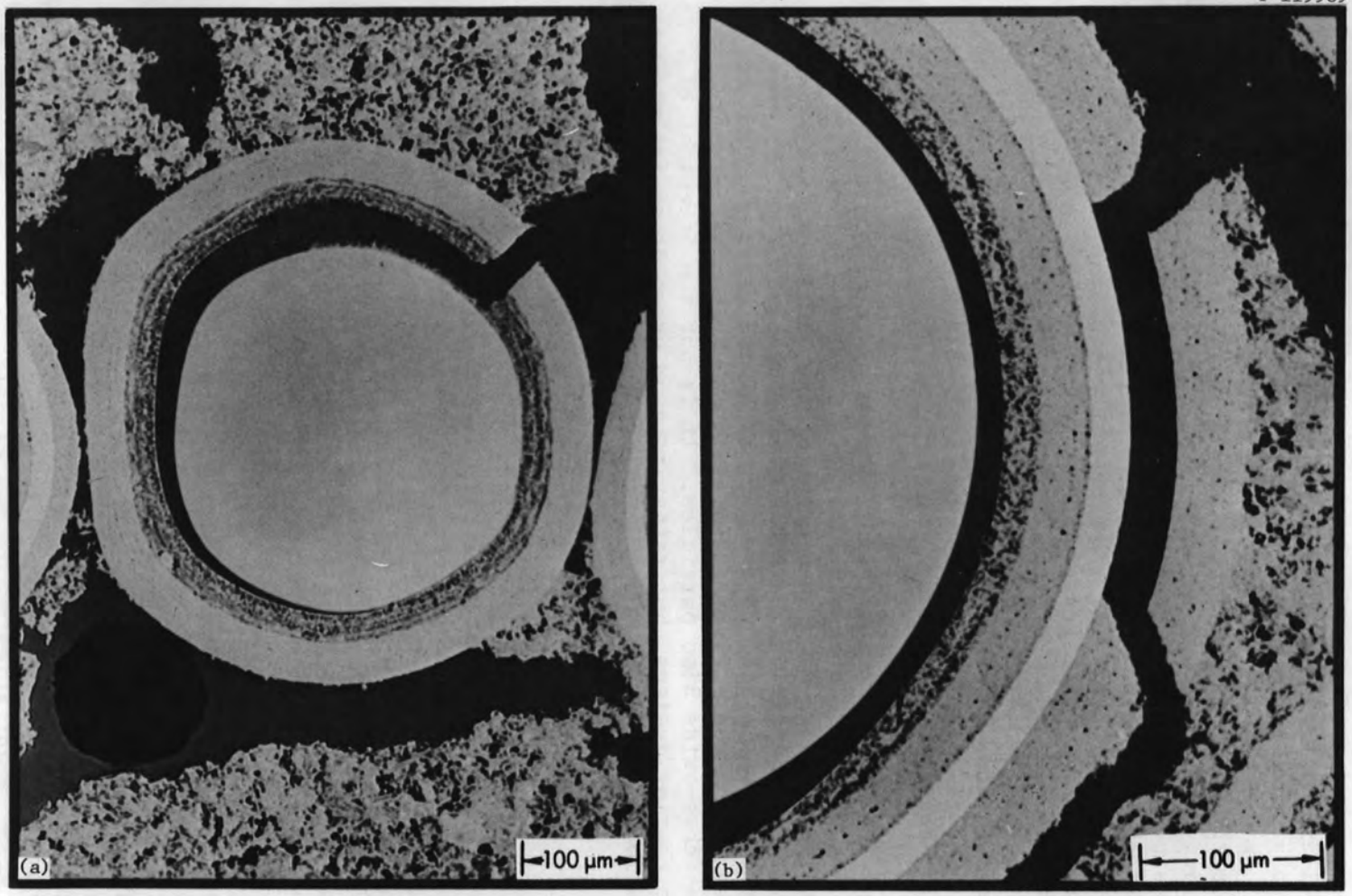

Fig. 23. Particles Broken During Irradiation Due to Matrix-Particle Interaction. Carbonized in graphite tube. Irradiated to 3.6×10^{21} n/cm^2 (E > 0.18 MeV) at 940–1145°C. (a) Biso particle. (b) Triso particle.

The causes of matrix-particle interaction are not yet fully understood. It is known that no single parameter is controlling, rather, it is a combination of matrix density, microporosity content, and pitch-coke yield. A comparison of the matrix structures for fuel rods irradiated in the OF-1 experiment[15] is shown in Fig. 24. No matrix-particle interaction problem was encountered in the fuel rods irradiated in OF-1.

From a thermal conductivity standpoint it is desirable to have a dense matrix. Therefore, work has been done to adjust the matrix materials and processing variables so that fuel rods can be manufactured with dense matrices, yet maintaining a high proportion of porosity as microporosity, as shown in Fig. 25. The appearances of the matrices produced by different carbonization techniques are more similar in Fig. 25 than was the case in Fig. 24. No problems with matrix-particle interaction have been encountered since the HRB-4 and -5 experiment; however, all in-block simulations have been conducted in graphite tubes. The characteristics of fuel rod matrices produced by in-block carbonization (on a production basis) are still unknown.

Examples of the irradiation performance of coated particles with fabrication defects are shown in Fig. 26. Four types of defects are shown in this figure: a missing segment of the SiC layer, a missing buffer layer, a nonspherical particle, and anistropic coating properties. The particles shown in Fig. 26 are not all of the same type and are not from the same fuel rod. Figure 26(a) is a WAR Triso particle; the others are dense-oxide Biso particles. It is not the intent of Fig. 26 to compare coating designs, but rather to give examples of failure due to fabrication defects.

FUTURE PLANS

The recycle fissile particles that have been developed for HTGR recycle application are adequate to survive the irradiation conditions of any HTGR application currently under consideration, including gas turbine and process heat HTGRs, for irradiation temperatures up to 1400°C. Further improvements in this design of these particles can be made to enhance the performance of other portions of the fuel system, notably the fuel rods and fuel elements. Fuel development work over the next few years can be divided into three categories:

1. development and irradiation testing in support of product specification development,
2. verification of the good performance of candidate fuels under real-time HTGR conditions, and
3. development of advanced fuels for gas turbine and process heat application. This work is primarily coating development and testing and improvements in the fuel rod to take advantage of the superior performance capabilities of the WAR kernels.

R-69222

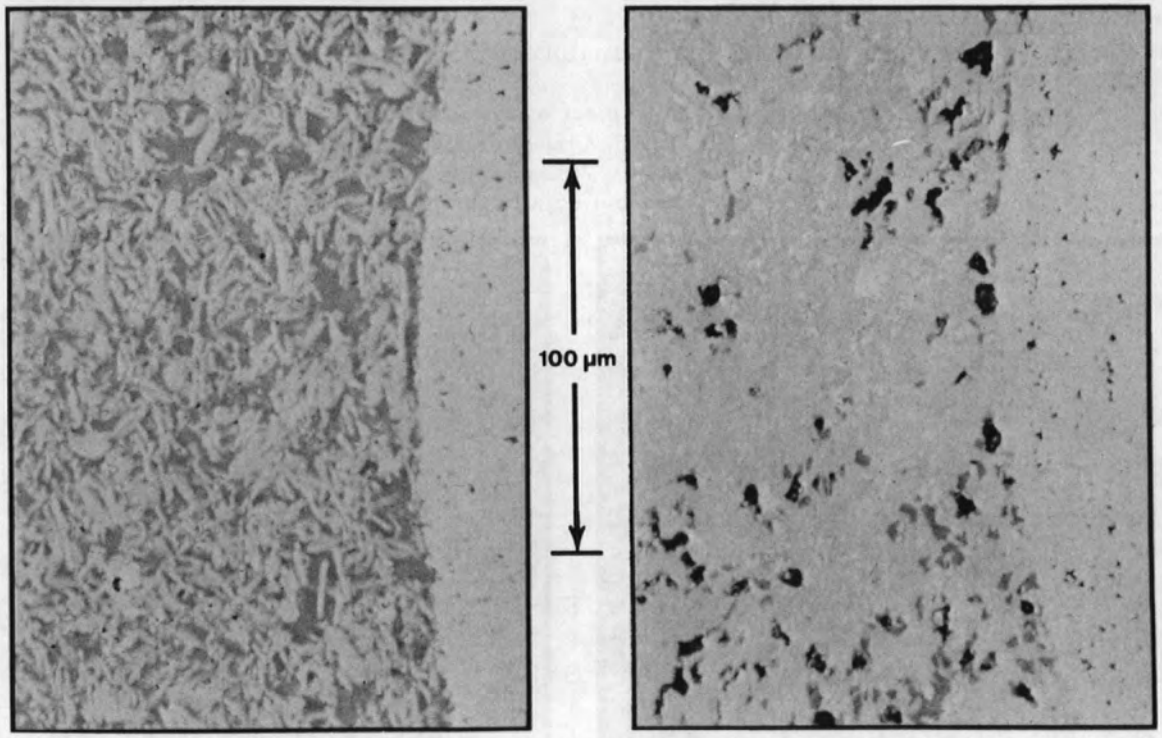

IN-PACKED ALUMINIA	CARBONIZATION MODE	IN-BLOCK
13.7	PITCH COKE YIELD (%)	44.9
41.6	MICROPOROSITY (%)	8.3
0.473	DENSITY g/cm^3	0.732

Fig. 24. Matrix Microstructures of Fuel Rods Irradiated in OF-1 Containing Asbury 6353 Filler (29 wt %) and Ashland A240 Pitch.

Y-119990

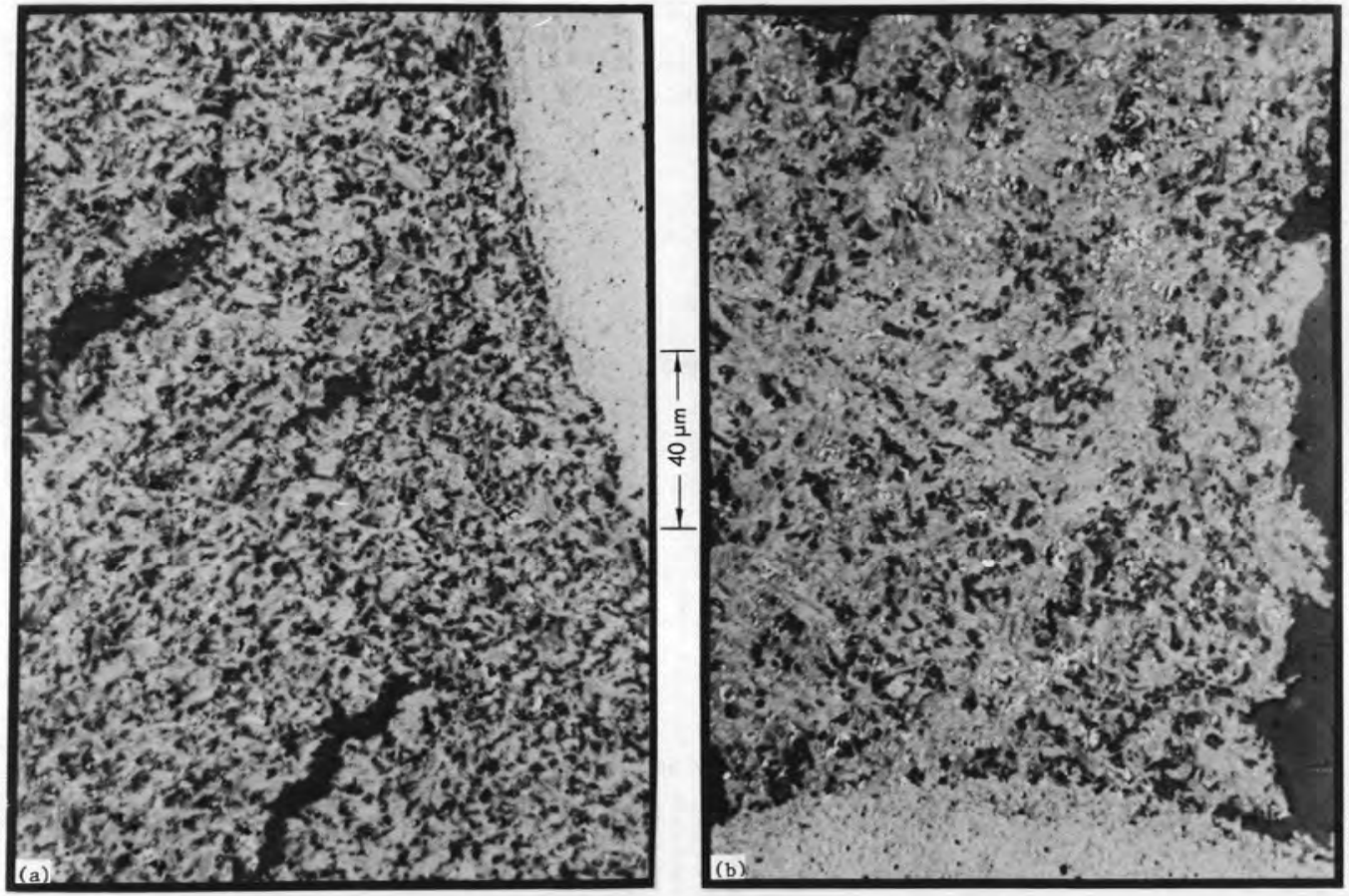

Packed Al_2O_3	Carbonization Technique	Graphite Tube
30	Microporosity (vol %)	24
0.75	Matrix Density (g/cm^3)	0.85
26	Pitch Coke Yield (wt %)	39

Fig. 25. Effect of Matrix Microstructure on Particle Breakage. (a) No broken particles. (b) Particles broken.

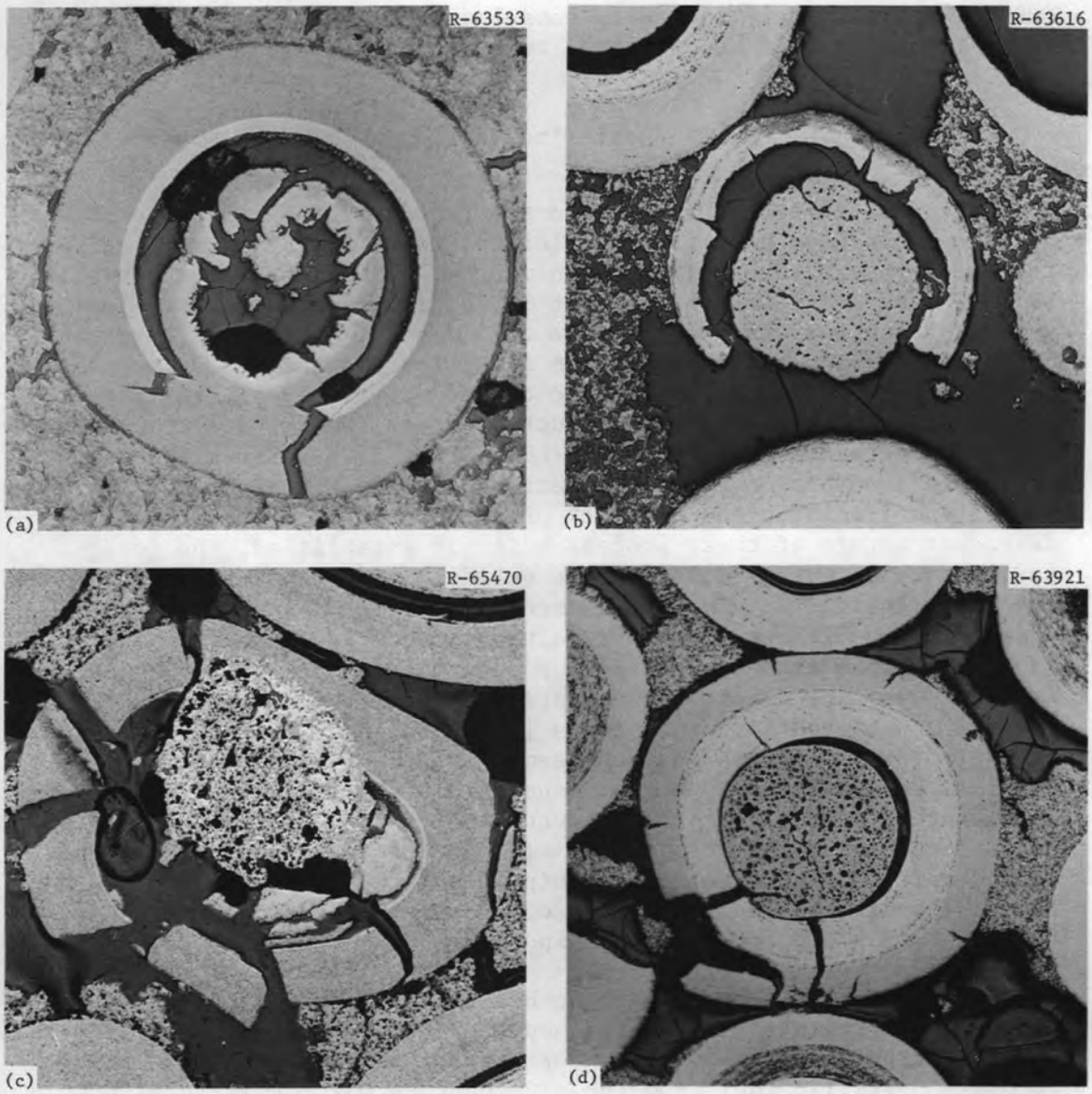

Fig. 26. Examples of Particles That Failed Because of Manufacturing Defects. 150×. (a) Portion of SiC missing. (b) Buffer missing. (c) Nonspherical particle. (d) Poor-coating properties.

Product Specification Support

Over the next few years the product specification work will center around irradiation testing in the HFIR and the Oak Ridge Research Reactor (ORR). Approximately four HFIR capsules per year and one ORR capsule every two years will be dedicated to establishing product specifications.

Real-Time Testing

All data collected to date on the irradiation performance of WAR-derived fuels have been from accelerated tests. HRB tests reach full fast-neutron exposure in about ten months, compared to four years in an LHTGR and six years in the Fort St. Vrain Reactor (FSVR). Tests in the ORR reach full exposure in about 15 months, while HFIR target (HT) capsule tests are fully exposed in about four months. Testing under accelerated conditions is believed to be conservative in that the fuel is subjected to higher power production rates (watts/particle) and higher temperature gradients than those listed in Table 1. However, there are a number of kinetic aspects to fuel performance, notably amoeba and fission product attack of the coatings. Since the time-dependent nature of these processes is not established, the good performance of these fuels must be verified under real-time conditions. The Peach Bottom recycle test elements (RTE)[14,16,17] were irradiated under HTGR conditions, but these elements received less than half the maximum neutron exposure and burnup anticipated for the LHTGR, and no WAR fuel was included in these tests. Many of the performance characteristics observed for other fuels [ThO_2, $(Th,U)O_2$, UC_2] in the RTEs have also been observed in these same fuels when irradiated under accelerated conditions. These observations provide confidence that accelerated testing data are relevant and that fuels that perform well under accelerated conditions will also perform well under real-time HTGR conditions. However, this point needs to be proven more convincingly by a direct comparison with current reference fuels irradiated to full burnup and fast-neutron exposure.

Plans for a direct comparison between 15- and 75%-converted WAR fuel, both irradiated in the ORR and in FSVR, have been made. The fuel for this experiment is already under irradiation in the OF-2 capsule in ORR.[18] Fissile fuel from the same batches will be irradiated in FSVR test elements 2, 4, and 6, presently scheduled to begin irradiation in the fall of 1977. Additional capsule tests (accelerated) and real-time tests (in FSVR) are scheduled in support of the cold prototype development and hot subsystems testing portions of the Thorium Utilization Program.

Advanced Fuels

Beginning in FY 1977, work will begin at ORNL on advanced fuel designs to exploit the performance capabilities of WAR kernels. This work will concentrate on minimizing the temperature difference between the kernels and the coolant. Development will include the testing of alternate coatings, of thinner and stronger coatings, of higher conductivity matrices, and of alternate processing conditions that will produce fuel rods of higher overall thermal conductivity.

DISCUSSION AND SUMMARY

Five failure mechanisms have been identified and discussed. Of these mechanisms, two are independent of kernel chemistry and design. Amoeba, a severe problem with dense-oxide fissile kernels, has not been a problem with carbide fuels in the temperature and temperature-gradient regions of interest for the HTGR. Amoeba has not been observed in WAR-derived fuels containing more than 15% UC_2. Chemical interaction, a severe problem for dense carbide fuels, has been controlled in WAR fuels by the proper proportioning of UO_2 and UC_2 content. Pressure vessel failure due to dimensional changes in the coatings is independent of kernel type; however, the WAR fuel is considerably less dense than dense oxide or carbide kernels (3 g/cm^3 for WAR fuel vs 10 g/cm^3 for dense oxide and 13 g/cm^3 for dense carbide fuel). Also, WAR kernels have been observed to shrink during irradiation, leaving a gap between the kernel and the coatings. This high-porosity kernel and the void between the kernel and coatings will surely combine to raise the kernel operating temperatures of the WAR fuel (relative to dense kernels at the same watt/particle). The high temperature and high porosity will lead to higher fission gas release and higher stresses on the coatings, which may result in the need to redesign the coatings and make them thicker.

Lindemer's thermodynamic analyses[1] suggest that kernel stoichiometries ranging from 15 to 70% conversion from oxide to carbide should perform well. In kernels with less than 15% carbide, the fission-released oxygen will react with carbon to form CO, which will raise the internal gas pressure and perhaps contribute to thermal migration as well as pressure vessel failure. Should the CO reach the SiC layer due to failure or permeability of the inner PyC, the CO will react with the SiC to form silicon oxides and ultimately fail the SiC layer. In kernels with more than 70% carbide, there is insufficient oxygen present to combine with the chemically active rare-earth fission products, which will migrate as carbides and attack the SiC and inner PyC layers. Irradiation testing to date supports the conclusions of the thermodynamic studies. Stoichiometries of 0, 15, 50, 75, and 100% carbide have been tested. The WAR UO_2 fuel probably exhibited excessive thermal migration. The WAR UC_2 fuel exhibited excessive fission product attack of the SiC layer causing a high failure fraction in these particles.

The 15, 50, and 75% carbide kernels performed well, with increasing rare-earth fission product loss from the kernels (attack of the SiC noted) as carbide content increased.

The kernel process development work done to date has indicated that the flexibility anticipated for WAR fuel, with respect to kernel density and stoichiometry, is indeed possible in laboratory-scale equipment. The technology appears to be capable of extrapolation to production-scale equipment with no difficulty. Additional work on process development will continue to determine process latitudes.

The importance of the work described in this report is that a fissile fuel has been developed which will perform well in any HTGR application currently under consideration — up to irradiation temperatures of 1400°C. It is anticipated that additional irradiation testing of optimum stoichiometries will further raise the temperature limit. Further, the processes required to produce these particles are readily adaptable to remote operation, which is essential for a recycle fuel. Direct comparisons of WAR-derived fuel with current reference fresh fuel (dense UC_2) suggest superior performance by the WAR fuel, which further suggests that the WAR fuel may become the reference fresh fissile fuel as well as the reference recycle fuel.

Future work should be directed at optimizing the WAR particle design and developing a product specification for manufacture. Additional work should be done to improve the fuel rod and fuel element design to take advantage of the performance capabilities of the coated particles. Design modifications that minimize the temperature difference between kernels and coolant will permit higher coolant temperatures, higher thermal efficiency, and more complete capabilities of the HTGR relative to the needs of steam cycle power production and process heat applications.

ACKNOWLEDGMENTS

The authors wish to acknowledge the entire HTGR staff for the significant contributions in the areas of planning, execution, and evaluation of the numerous irradiation experiments over the past decade. In particular, the authors wish to acknowledge P. R. Kasten, J. H. Coobs, A. L. Lotts, W. P. Eatherly, J. L. Scott, J. D. Sease, R. A. Bradley, R. B. Fitts, A. R. Olsen, and R. L. Beatty of the Metals and Ceramics Division and J. A. Conlin, B. H. Montgomery, and K. R. Thoms of the Reactor Division for their participation in the planning and designing of the experiments; the individuals in the Metals and Ceramics Division that participated in the fabrication and characterization of the test particles and fuel rod specimens: R. L. Hamner, J M Robbins, W. J. Lackey, A. J. Caputo, G. W. Weber, C. B. Pollock, W. H. Miller, Jr., C. Hamby, D. E. Rosson, J. B. Flynn, and C. E. DeVore. The dosimetry and thermometry of the capsules were provided by H. T. Kerr of the Reactor Division and R. L. Shepard of the Instrumentation and Controls Division, respectively.

Thanks go to T. N. Tiegs and E. L. Ryan of the Metals and Ceramics Division for the conduction of the postirradiation examinations of the more recent experiments and to E. M. King and his staff of the Operations Division for their assistance in providing the facilities and services required to conduct postirradiation examinations. The metallography of the unirradiated controls was performed by M. D. Allen of the General Metallography group, and the remote metallography was performed by N. M. Atchley and L. G. Shrader of the Radiation and Electron Metallography group of the Metals and Ceramics Division. The electron microprobe analyses were performed by T. J. Henson of the Radiation and Electron Metallography group of the Metals and Ceramics Division. The authors also acknowledge the technical reviews and constructive comments provided by T. B. Lindemer and G. W. Weber, and the assistance of R. H. Powell, Jr., for technical editing and Julia Bishop for typing and makeup of the report.

REFERENCES

1. F. J. Homan et al., "Development of a Recycle Fuel for the HTGR," paper submitted to *Nuclear Technology*.

2. J. A. Conlin et al., "HTGR Fuel Irradiations and Postirradiation Examinations," pp. 90–97 in *Gas-Cooled Reactor Programs Annu. Progr. Rep. Dec. 31, 1973*, ORNL-4975.

3. J. D. Sease, "Fuel Fabrication Process Development," pp. 33–56 in *Gas-Cooled Reactor Programs Annu. Progr. Rep. Dec. 31, 1972*, ORNL-4911.

4. Preliminary Safety Analysis Report for Fulton Generating Station, Chap. 4.

5. Preliminary Safety Analysis Report for Summit Generating Station, Chap. 4.

6. T. B. Lindemer and R. L. Pearson, *Kernel Migration for HTGR Fuels from the (Th-U-C-O-N) System*, ORNL/TM-5027 (April 1976).

7. O. M. Stansfield et al., "Kernel Migration in Coated Carbide Fuel Particles," *Nucl. Technol.* 25: 517–30 (1975).

8. *National HTGR Fuel Recycle Development Program Plan*, prepared by Oak Ridge National Laboratory and Gulf General Atomic, ORNL-4702 (August 1971), p. 16.

9. J. L. Scott et al., *An Irradiation Test of Bonded HTGR Coated Particle Fuels in an Instrumented Capsule in HFIR*, ORNL-TM-3640 (March 1972).

10. R. A. Olstad et al., *An Irradiation Test of Candidate HTGR Recycle Fuels in the H-1 and H-2 Capsules*, ORNL-TM-4397 (July 1974; Addendum, April 1975).

11. K. H. Valentine et al., *Irradiation Performance of HTGR Fuel Rods in HFIR Experiments HRB-7 and -8*, in preparation.

12. F. J. Homan et al., *Irradiation Performance of HTGR Fuel Rods in HFIR Experiments HRB-4 and -5*, ORNL-5115 (June 1976).

13. F. J. Homan et al., *Irradiation Performance of HTGR Fuel Rods in HFIR Experiments HRB-9 and -10*, in preparation.

14. E. L. Long, et al., *Fabrication of ORNL Fuel Irradiated in the Peach Bottom Reactor, and Postirradiation Examination of Recycle Test Elements 7 and 4*, ORNL-TM-4477 (September 1974).

15. T. N. Tiegs et al., *Irradiation Performance of HTGR Fuel Rods in ORR Experiment OF-1*, in preparation.

16. R. B. Fitts, "Recycle Test Elements in the Peach Bottom Reactor," pp. 126–33 in *Gas-Cooled Reactor Programs Annu. Progr. Rep. Dec. 31, 1972*, ORNL-4911.

17. J. A. Conlin et al., "HTGR Fuel Irradiations and Postirradiation Examinations," pp. 89–172 in *Gas-Cooled Reactor Programs Annu. Progr. Rep. Dec. 31, 1973*, ORNL-4975.

18. *HTGR Base Program Progress Report for January 1, 1974, through June 30, 1975*, ORNL-5108, Chap. 6 in preparation.

ORNL/TM-5502
UC-77 (Gas-Cooled
Reactor Technology)

INTERNAL DISTRIBUTION

1–3. Central Research Library
4. Document Reference Section
5–14. Laboratory Records Department
15. Laboratory Records, ORNL RC
16. ORNL Patent Office
17. R. L. Beatty
18. R. A. Bradley
19. A. J. Caputo
20. J. A. Conlin
21. J. H. Coobs
22. D. Costanzo
23. F. L. Culler
24. R. G. Donnelly
25. W. P. Eatherly
26. R. B. Evans III
27. J. I. Federer
28. R. L. Hamner
29. R. F. Hibbs
30–32. M. R. Hill
33–37. F. J. Homan
38. D. R. Johnson
39. M. J. Kania
40–41. P. R. Kasten
42. H. T. Kerr
43. W. J. Lackey
44. T. B. Lindemer
45–47. E. L. Long, Jr.
48. A. L. Lotts
49. R. E. MacPherson
50. B. H. Montgomery
51. C. S. Morgan
52. M. T. Morgan
53. K. J. Notz
54. R. L. Pearson
55. W. H. Pechin
56. H. Postma
57. W. W. Proaps
58. J M Robbins
59. J. D. Sease
60. R. L. Shepard
61. T. N. Tiegs
62. K. R. Thoms
63. K. H. Valentine
64. G. W. Weber
65. J. R. Weir, Jr.
66. P. M. Brister (consultant)
67. John Moteff (consultant)
68. Hayne Palmour III (consultant)
69. J. W. Prados (consultant)
70. N. E. Promisel (consultant)
71. D. F. Stein (consultant)

EXTERNAL DISTRIBUTION

72–73. ERDA DIVISION OF NUCLEAR FUEL CYCLE AND PRODUCTION, Washington, DC 20545

Director

74–75. ERDA DIVISION OF NUCLEAR RESEARCH AND APPLICATION, Washington, DC 20545

Director

76–77. ERDA OAK RIDGE OPERATIONS OFFICE, P.O. Box E, Oak Ridge, TN 37830

Director, Reactor Division
Director, Research and Technical Support Division

78–244. ERDA TECHNICAL INFORMATION CENTER, Office of Information Services, P.O. Box 62, Oak Ridge, TN 37830

For distribution as shown in TID-4500 Distribution Category, UC-77 (Gas-Cooled Reactor Technology)

☆ U.S. GOVERNMENT PRINTING OFFICE: 1976-748-189/450